APCC
APEC CLIMATE CENTER

TECHNICAL REPORT

APCC
APEC CLIMATE CENTER

PREFACE

It is our pleasure to present to you the APEC Climate Center (APCC)'s Technical Report 2012, which reports the core outcomes of our research activities from the past year.

Since 2005, APCC, as a hub of climate information in the Asia-Pacific region, has strived to share our analysis and prediction of abnormal climate and to apply this information to regional development. The Center has established the most extensive Multi-Model Ensemble (MME) system for seasonal prediction in the world through its international science network and has provided value-added products to various stakeholders. Recently, APCC has expanded its mandate to include enhancing the capacity of APEC member economies to respond effectively to climate change and variability through better application of climate information.

In 2012, APCC continued to make an effort to improve the quality and quantity of our short-term climate forecasts and our online climate information systems, as information dissemination tools. Additionally, APCC began its endeavor to produce more applicable climate information through interdisciplinary research among various sectors, such as agriculture and hydrology. The following technical report provides more information about our research outcomes from 2012.

In 2013, following APCC's goal to enhance socioeconomic well-being through better utilization of climate information, APCC will continue to improve the quality and accuracy of its climate information, recognizing that the utility of this information is only as good as its quality. We would like to make the best use of our research outcomes in various scientific and application areas. We welcome any feedback on this report or on our services.

My best and warmest regards to all of you.

Dr. Chin-Seung Chung
Director/APEC Climate Center

CONTENTS

APCC

TECHNICAL REPORT 2012-03

Climate Change Projection over South Asian Summer Monsoon using CMIP5 Coupled Climate Models

Dr. Venkatraman Prasanna

ASSESSMENT OF SOUTH ASIAN SUMMER MONSOON SIMULATION IN THE HISTORICAL RUN OF CMIP5 COUPLED CLIMATE MODELS

ABSTRACT

This paper evaluates the performance of 29 state-of-the-art CMIP5 coupled atmosphere-ocean general circulation models (AOGCM) in their representation of the regional characteristics of monsoon simulations over South Asia. Despite their relatively coarse resolution, the AOGCMs have shown some skill in simulating the mean monsoon and precipitation variability over the South Asian monsoon region. However, considerable biases exist with reference to observed precipitation and inter-model differences are apparent. The models are evaluated for the ENSO-monsoon teleconnection and the veracity of modeled air-sea interactions in the Indian Ocean during the summer monsoon season. The monsoon rainfall and surface flux bias, with respect to observations from the historical run (for the period 1850 to 2010), are discussed in detail. Our results show that the coupled model simulations over South Asia exhibit large uncertainties between models. The analysis clearly exhibits the presence of large systematic biases in the coupled simulations of boreal summer precipitation, evaporation, and sea surface temperature (SST) in the Indian Ocean, often exceeding 50% of the climatological values, and such biases are common to many of the models. Overall, the coupled models are found to be deficient in portraying the boreal summer monsoon over the South Asian monsoon region, and it is therefore apparent that they need further improvement.

1. INTRODUCTION

The climate of South Asia is dominated by the monsoons. During the summer monsoon season from June to September (JJAS), most parts of India receive the major proportion (75% to 90%) of their annual rainfall. The amount of rainfall increases by almost three orders of magnitude from west to east across the Indian subcontinent during the monsoon period and devastating floods are a common feature. Simultaneous drought can also occur in other areas of the subcontinent. The summer monsoon rainfall, (a dependable source of water for the country), has been evidenced by a remarkable large-scale stability in more than a century of recorded data (with a coefficient of variation of 10%), and with a variety of temporal and spatial variations (Pant and Rupa Kumar, 1997). While a large part of the seasonal anomalies in the

monsoon are accounted for by interannual variability, decadal and longer term changes manifest themselves as changing frequencies of extreme anomalies. Such changes are, therefore, of crucial importance for providing resources during flood or drought calamities.

It is now a well-established fact that General Circulation Models (GCMs) are successful in depicting the gross features of observed large-scale climatological features. GCMs have also projected changes in the global climate due to increasing greenhouse gases over the 20th and 21st centuries (in the Intergovernmental Panel on Climate Change (IPCC) scientific assessment reports (IPCC 1996, 2001, 2007; Christensen *et al*. 2007)). However, as GCMs are yet to realistically reproduce observed features on a regional scale, there is a large uncertainty associated with regional projections, particularly over the monsoon region (Prasanna and Yasunari, 2011). The skill of atmospheric GCMs (AGCMs) forced with observed sea surface temperatures (SSTs) in simulating the Asian summer monsoon has been fairly static (Kang *et al*. 2004; Wang *et al*. 2004), with large systematic biases in the simulations (Kang *et al*. 2002). Coupled atmosphere-ocean GCMs (CGCMs) also show large model-to-model variability and discrepancies, compared with observations (Covey *et al*. 2003; Meehl *et al*. 2005). The monsoon precipitation simulations in the IPCC-AR4 CGCMs show problems in simulating the seasonal mean and interannual variability of the Asian summer monsoon (Prasanna and Yasunari, 2011; Ueda *et al*. 2006; Annamalai *et al*. 2007; Kripalani *et al*. 2007). These models also have deficiencies in capturing the air sea interaction over the tropical Indian Ocean (Wu *et al*. 2006, 2007; Lin 2007; Wu and Kirtman 2007; Bollasina and Nigam, 2008). Examination of the performance of seven fully coupled models participating in the "Development of a European Multimodel Ensemble system for seasonal to inTERannual prediction" (DEMEMER) program revealed that the large biases in the predicted SSTs over the Indian Ocean region and the inadequate monsoon teleconnection simulations (IODM-monsoon, ENSO monsoon) are the possible reasons for the coupled models' lower skill in the simulation of monsoon rainfall (Preethi *et al*., 2010). Most coupled models participating in the ENSEMBLE EU projects are characterized by an excessive oceanic forcing in the atmosphere over the equatorial Indian Ocean. Furthermore, the models could not capture the recent weakening of the ENSO-Indian monsoon relationship.

They could, however, correctly capture the north Atlantic-Indian monsoon teleconnection, which is independent of the ENSO (Rajeevan *et al.*, 2011).

Climatic variations and change caused by external forcings may be partly predictable, particularly on larger spatial scales (e.g. continental and global scales). It is evident that human-induced increased emissions of greenhouse gases have resulted in external forcings, and it is believed that these large-scale aspects of human-induced climate change are also partly predictable. Nevertheless, it is clear that uncertainties in the models' simulations for the historical period (1850–2010; present climate) need to be studied in detail and validated before the models can be used for future climate projections. The model bias calculated with respect to observations is the systematic bias present in the each model. Each model bias calculated with respect to the observations acts as additional information and promotes the use of caution for the interpretation of future climate change projections from multi-model simulations. By excluding models with a large bias over a selected domain of interest and by removing models with large systematic bias (model errors) it may, however, be possible to obtain reliable future climate change projections.

This paper focuses mainly on the model bias in the mean and variability in the CMIP5 historical run. To have a reliable projection based on coupled model results, the models need to be able to capture the observed features of the monsoon in the historical run. These features are as follows: 1) the mean, 2) the variability and 3) the global teleconnections. The models are tested for a present-day simulation of seasonal mean precipitation (during JJAS). The bias with respect to the observations and the processes responsible for the precipitation bias, are also discussed in detail. The year-to-year spatial variability of each model is compared with the observed year-to-year spatial variability. The models' ability to capture the observed significant teleconnection patterns is also tested.

The structure of this paper is as follows: Section 2 describes the observed and model datasets used; Section 3 discusses the observed and simulated South Asian monsoon features, presents a discussion on the simulated variability of the monsoon by CGCMs, and discusses the teleconnection patterns in the observation and models; and Section 4 presents the discussion and main conclusions.

2. METHODOLOGY

2.1 Data and Experiment

2.1.1 Observational Datasets

The period of analysis nominally covers the summer monsoon season of June-July-August-September (JJAS) for the years 1870 to 2010. The data products used are the Global Precipitation and Climatology Project (GPCP) precipitation (Adler *et al*., 2003), the monthly All India Summer Monsoon Rainfall index (Parthasarthy *et al*. 1994), the monthly fields of surface winds (U,V), precipitable water (PRW), evaporation (LHF) obtained from NCEP/National Center for Atmospheric Research (NCAR), the 20th reanalysis dataset (Compo *et al*. 2011), and the monthly Sea Surface Temperature (SST) for the period 1870–2010 from HADISST (Hadley Center optimum interpolated SST dataset) (Rayner *et al*., 2003). The 20th century reanalysis precipitation closely follows the AISMR index prepared from the IITM data (figure not shown) and the highest spatial grid correlation from the GPCP over the core monsoon region. Only a few regions such as the Himalayan and northwest desert regions show less correlation during the period 1979–2008 (figure not shown). Since the 20th century datasets are available for the same length of time as the model datasets, we used the 20th century datasets for model intercomparisons.

2.1.2 Model Datasets

Transient climate change simulations of 29 CGCMs were used in the present study, and are part of the suite of simulations performed for the CMIP5 intercomparison studies and the IPCC AR5 scientific assessment report. The main centers of development of the 29 models used in the study, along with their acronyms, are listed in Table 1. Technical details of the above AOGCMs, including the resolution and various model components, together with the length of simulation, are also summarized in the table. The 29 models were tested to simulate global climate representing the present climate using the historical run. Monthly data of precipitation,

evaporation, precipitable water and winds (U.V) from CGCMs (Table. 1) were utilized in this study. The length of the data for each model run was nominally 160 years of simulation, to correspond with the present climate of 1850–2010.

2.1.3 Model Experiment

For the simulation experiment in this study we used the historical run, which is a control integration in which the atmospheric forcing, in terms of the greenhouse gas concentration, is taken from a reconstructed time series of concentrations and performed for a period of roughly 150 years, typically 1850–2010. In each model, the climatology is constructed from the historical run to represent the present day climate (1850–2010).

3. RESULTS

3.1 Observed and CGCM simulated monsoon over South Asia

3.1.1 Climatological mean monthly Annual Cycle

Climatological mean observed annual cycle using the GPCP data and the simulated climatological mean annual cycle of the model for precipitation are shown in Fig.1. Precipitation is averaged over the South Asian region (land and sea) comprising 5°N-35°N and 65°E-95°E. The simulated precipitation shows a remarkably similar pattern to that of the observed. The amount of precipitation varies from less than 2 mm/day during the January-April period to more than 6 mm/day during the peak summer monsoon period of June-August. The annual cycle is thus characterized by a sharp increase from April to June and thereafter a gradual decrease from September. Examination of the models' simulations (Fig. 1) suggests that most models capture both the shape and magnitude well with respect to the observation. The results are summarized as follows:

i) Seven models simulated a similar annual cycle in terms of shape and magnitude to those of the observed characteristics. They are: Can-ESM, FGOAL-s2, GISS-E2-H, GISS-E2-R, HADCM3, HADGEM2-CC, and HADGEM-ES.

ii) Ten models simulated a similar shape of annual cycle, but simulated excess precipitation during the summer. They are ACCESS, BCC, CCSM4, FGOAL-g2, MIROC-4H, MIROC-5, MIROC-ESM-CHEM, MIROC-ESM, MPI-ESM-LR, and MPI-ESM-P.

iii) Six models simulated the shape of the annual cycle, but underestimated the precipitation amounts; particularly in the spring and summer periods. They are: CNRM-CM5, CSIRO-MK3, IPSL-CM5A-LR, IPSL-CM5A-MR, IPSL-CM5B-LR, and MRI-CGCM3.

iv) Six models simulated peak rainfall one month later than that of the observed period, resulting in the underestimation of rainfall during spring and summer. They are: GFDL-CM3, GFDL-ESM2G, GFDL-ESM2M, INMCM, NOR-ESM-ME, and NORESM-M.

3.1.2 Observed and Model simulated interannual variability and epochal signatures

India has an excellent network of instrumental records extending for more than a century. Based on such a long period of instrumental records, several studies in the past have indicated that the All-India Summer Monsoon Rainfall' (AISMR) series does not show any significant long-term trend during the instrumental record (spanning more than 150 years) (Fig. 2a). However, it does exhibit a distinct epochal behavior (Fig. 2(b),(c)) on a low frequency time scale of 3 to 4 decades, characterized by alternating periods of higher and lower frequencies of deficient rainfall years (Pant and Kumar, 1997).

The simulated interannual variability and the epochal signature of the models are shown in Figs 3, 4 and 5. The observed interannual variability of AISMR has a mean of around 848 mm and a departure of +/- 84mm (Fig. 2a), whereas the simulated model mean precipitation varies from 300 mm to 1200 mm (Fig. 3). To identify whether the models are able to capture the observed epochal behavior, the

31-year running mean (Fig. 4) and the 31 year running standard deviations (Fig. 5) are prepared similar to the observed (Fig. 2(b)(c)). Most of the models failed to capture the observed epochal signatures of the mean, with the exception of a few models, namely: ACCESS, FGOAL-g2, and HADGEM-CC (but with a lower mean than the observed) as shown in Fig. 4. Unlike the mean, the epochal signature in the standard deviations is captured in the model number of the models, namely ACCESS, MIROC 5, and NOR-ESM-ME. Although the other models, FGOAL-g2, FGOAL-s2, HADGEM-CC, and INMCM produce an epochal-nature, this nature does not coincide with the observed pattern (Fig. 5).

3.1.3 Identifying better performing models

In order to identify the best performing models over South Asia, the model simulated climatological mean and CV averaged over 5°N-35°N and 65°E-95°E were scattered along with the observed climatological mean and CV and calculated over the same domain as that of the GPCP data (Fig. 6). The best performing models were chosen by selecting those with results falling close to those of the observed. Models such as GFDL-ESM2M, NMCM, MPI-ESM-P, and FGOAL-g2 produced a similar mean and CV to the observed. However, even when the mean and CV were relaxed by 10 to 20%, only 50% of the models (14 models) could be selected to make projections. Out of the 29 participating models, only 50% were close to the observation. It should be considered here that this simulation was on an area averaged over a large domain in South Asia, and if the models had been tested over a much smaller domain then large uncertainties would have been apparent. In the following sections the model errors and processes responsible are discussed.

3.1.4 Simulation of spatial mean summer monsoon precipitation and systematic bias in the modeled precipitation

The climatological spatial mean from JJAS is shown in Fig. 7. The first panel shows the 30-year climatological mean for JJAS from the GPCP observation. The subsequent 29 panels show the model simulated JJAS climatological mean. The

precipitation amount varies from 2 mm/day to 16 mm/day over the Indian region. The heavy precipitation over north-east India is simulated well in most models, but most models fail to produce the heavy precipitation over the south-west region (over the Western Ghats) in the Indian peninsular. Most models simulate the observed precipitation maximum over the equatorial Indian Ocean either too heavily or too lightly, and many models fail to even simulate the observed shape of the maximum-minimum spatial pattern observed over South Asia. The three regional heat sources (Annamalai and Sperber, 2005) observed over (1) the Indian region, (2) the equatorial Indian Ocean, and (3) the Philippine Sea, are either underestimated or overestimated in most models.

The model precipitation bias with respect to the observation (GPCP) is shown in Fig. 8; the first panel is the observed climatological mean from the GPCP observation. Most models show a negative bias in precipitation over the South Asian monsoon region during the summer monsoon period (JJAS), except for a few models which show a positive bias over a large part of South Asia, namely, CCSM4, MIROC-4H, MIROC-5, MIROC-ESM, and MIROC-ESM-CHEM. The models showing a strong negative bias are HADCM3, HADGEM-CC, HADGEM-ES, IPSL-CM5A-LR, IPSL-CM5A-MR, IPSL-CM5B-LR, MRI-CGCM3, and CSIRO-MK3.

The models simulate either a high precipitation bias or a low precipitation bias due to the systematic bias in the processes within the models responsible for the generation of precipitation. The important aspects, or variables, of precipitation generation are discussed in the following section.

3.1.5 Processes responsible for systematic model errors (bias)

The most important variables responsible for precipitation generation were examined for their systematic errors in each model, using the model's simulation of precipitation over the South Asian domain. Since the monsoon is a coupled process (Land-Ocean-Atmosphere coupling), the models were examined for SST, Evaporation and Wind in their ability to simulate a realistic representation of the local air-sea interaction over the Indian Ocean sector. This area of investigation was chosen because local air-sea

interactions over the Indian Ocean play an important role in shaping the monsoon over the South Asian sub-continent. Biases in the following variables are described as follows:

Bias in the Sea Surface Temperature (SST):

The most fundamental aspect of precipitation anomalies was found in those of SST. The models were therefore examined for a SST-bias (Fig.9) in their ability to simulate SST anomalies over the Indian Ocean, as SST contributes to precipitation through an air-sea interaction. Most models produced a cold SST bias over the Indian Ocean sector, except for a few, namely: CCSM4, GISS-E2-H, GISS-E2-R, HADCM3, INMCM, IPSL-CM5A-MR, MIROC-4H, and this implies that the models would therefore simulate the production of less precipitation, causing a reduction in the hydrological cycle.

Bias in the Evaporation/Latent heat flux (LHF):

Evaporation is the result of surface hydrological processes, and the inclusion of evaporation in land and ocean models results in changes in albedo, emissivity and surface-atmosphere energy interchanges. A bias in evaporation could be due to either a bias in the land/ocean model, or in the model interface.

Increased (decreased) evaporation due to higher (lower) SST and land temperatures can result in higher (lower) precipitation. The bias in evaporation was found through air-sea interactions or through the air and land interface. It is also noted (figure not shown) that most models produced a cold land-temperature bias. This could be due to poor representation of land surface processes within the land models of the respective CGCMs. A negative evaporation bias was found over South Asia in 50% of the models (Fig. 10).

Bias in the Column Integrated Water Vapor or Precipitable water (PRW):

As temperatures increase over land and ocean, the water vapor content of the atmosphere increases, through an increase in evaporation. A warm (cold) SST or land temperature bias will result in enhanced (suppressed) precipitable water content. Most models show a negative precipitable water content (Fig. 11) over South Asia, which introduces a significant uncertainty in the models' simulations.

A positive feedback mechanism occurs with the increase (decrease) of atmospheric water vapor resulting from increased (decreased) evaporation as a response to an

increase (decrease) in temperature. PRW causes greenhouse warming of the surface as a result of the absorption of infrared radiation emitted from the Earth's surface. The greenhouse effect created by the excess (reduced) water vapor results in the temperature increase (decrease), and as the temperature rises (falls) the atmosphere is able to hold more (less) water vapor. Precipitable water is, therefore, an important variable and it is desirable for it to be realistically represented without bias for the monsoon in order to project accurate regional climate change using CGCMs.

Bias in the Zonal and Meridional Winds (U, V):

Winds are a dynamical response to atmospheric heating. When the models fail to represent the monsoonal heating, the bias will therefore be reflected in the dynamical response of the atmosphere in the creation of winds. The climatological wind pattern during the monsoon season (JJAS) is shown in Fig. 12. It is evident that most models produced the cross equatorial flow (south westerlies), but with differing magnitudes. The wind components are split into zonal and meridional components and bias is calculated with respect to the 20th century reanalysis wind climatology for the JJAS season. The zonal winds represented are the mean westerlies over South Asia, with a peak strength of around 10 m/sec (Fig. 13) in the Arabian sea sector. Most models produce weak westerlies and the negative bias varies from -1 m/s to -5 m/s. The meridional winds represented are the mean southerlies over South Asia, with a peak strength of around 8 m/s to 10 m/sec (Fig. 14) along the Somali coast. It is evident from Fig. 14 that most models produce weak southerlies and that the negative bias varies from -1 m/s to -5 m/s.

3.1.6 Simulated spatial variability of South Asian monsoon by CGCMs

Apart from changes in the climatological mean state, the monsoonal year-to-year variability, (otherwise known as interannual variability) has a profound impact on various human activities and can lead to large-scale drought and floods. In view of this, the models were examined for the spatial pattern of the variance (standard deviation) of monsoon rainfall in comparison with the observed variance (standard

deviation) in the 20th century reanalysis data. The standard deviation is taken here to represent the variance of the rainfall and is computed for a period of 140 years (1870–2010) from the 20th century data and during the entire period of simulation for the models. The results are presented in the form of bias with respect to the 20th century reanalysis standard deviation over each grid for every model respectively (Fig. 15). Most models in the historical simulation showed a general tendency of decreased variance compared with the 20th century reanalysis over South Asia. However, a few models showed a large systematic increase in variance compared with that of the observation, namely, ACCESS, FGOAL-g2, FGOAL-s2, GFDL-ESM2M, IPSL-CM5A-MR, IPSL-CM5b-LR, MIROC-4H, and MIROC-5.

3.1.7 Global teleconnection pattern in the observation and CGCMs over South Asia

Observational data from over more than a century shows clear evidence of the association between a weak monsoon and El Niño events (Pant and Parthasarathy, 1981). During the period 1871–2002, 11 out of a total of 23 drought years were El Niño years (Rupakumar *et al*., 2003). The impact of the El Niño/Southern Oscillation (ENSO) on the South Asian summer monsoon has been explored intensively (Rasmusson and Carpenter, 1983; Krishna Kumar *et al*., 1999; Ailikun and Yasunari, 2001; Chang *et al*., 2001; Kawamura *et al*., 2005). The El Niño years are generally associated with below-normal South Asian summer monsoon rainfall (Rasmusson and Carpenter, 1983; Yasunari, 1990).

To show the teleconnection patterns of the All India Summer Monsoon Rainfall (AISMR) with the global SST, the Hadley center optimum interpolated global SST (HADISST) (1870 – 2010) for JJAS was correlated with the selected All India domain's JJAS precipitation (5N-35N; 65E-95E) from the 20th century reanalysis dataset (shown in the first panel of Fig. 16). A significant negative correlation (significant at 95%) over the Nino-3.4 region and a significant positive correlation (significant at 95%) over the Indian Ocean, Northwest Pacific and Atlantic regions, is evident. A similar procedure was performed for each model by taking the All India domain's JJAS precipitation (5°N-35°N and 65°E-95°E) from the model precipitation dataset and correlating it with the model's SST field. A few models succeeded in simulating the

observed pattern (but with stronger correlations), namely: BCC, CCSM4, GFDL-CM3. GFDL-ESM2M, GISS-E2-R, MIROC-5, MPI-ESM-LR. A few models simulated an additional negative SST relationship over the Indian Ocean sector, namely: ACCESS, CAN-ESM,CNRM-CM5, GISS-E2-H, HADCM3, HADGEM2-CC, HADGEM2-ES, IPSL-CM5A-LR, IPSL-CM5A-MR, IPSL-CM5B-LR, NOR-ESM-ME, NOR-ESM-M. A few models failed to capture the observed teleconnection at all, namely: FGOAL-g2, FGOAL-s2, MIROC-ESM-CHEM, MIROC-ESM, MRI-CGCM3.

Similarly, in order to understand the impact of the Niño 3.4 Index SST anomaly on global precipitation, the Niño 3.4 index precipitation from the HADISST was averaged over 5°S-5°N and 170°W to 120°W and correlated with the 20th century reanalysis global precipitation (Fig. 17). A significant positive correlation (significant at 95%) was seen over the entire Pacific region and a significant negative correlation (significant at 95%) over the Indian monsoon region, Maritime continental regions and Atlantic regions. Most models simulated the observed pattern, but with stronger correlations, namely: ACCESS, BCC, CAN-ESM, CCSM4, CNRM-CM5, GISS-E2-H, HADCM3, HADGEM2-CC, HADGEM2-ES, IPSL-CM5A-LR, IPSL-CM5A-MR, IPSL-CM5B-LR, NOR-ESM-ME, NOR-ESM-M, GFDL-CM3. GFDL-ESM2M, GISS-E2-R, MIROC-5, MPI-ESM-LR. A few models failed to capture the observed teleconnection, namely: FGOAL-g2, FGOAL-s2, MIROC-ESM-CHEM, MIROC-ESM, MRI-CGCM3.

4. DISCUSSION

4.1 Discussion and Conclusion

This paper provides a detailed discussion on the observed attributes of the South Asian summer monsoon and evaluates the performance of 29 state-of-the-art coupled atmosphere-ocean general circulation models (CGCMs) in their representation of the regional characteristics of rainfall over the South Asian summer monsoon region. It also discusses the models' biases in comparison with the observation and the processes shaping the generation of precipitation. The CGCMs, despite their relatively

coarse resolution, have shown a reasonable skill in simulating the South Asian monsoon. However, considerable biases do exist in comparison with the observation, and inter-model differences are quite large. These findings should, therefore, be taken into account when interpreting the models' simulations. Most of the models underestimated the South Asian monsoon due to systematic bias in their simulation, and most failed to simulate the higher SST's over the Indian Ocean as seen in the observations. The cold SST bias coupled with the poor air-sea interaction indicates an underperformance by most of the models over the South Asian Monsoon region. This underperformance of most of the coupled-models can be explained by their inability to adequately simulate the evaporative fluxes and resultant winds over the South Asian monsoon region. Most of the systematic bias in the models may arise from the different components of the model. For instance, the cold SST bias could be attributed to either a poor representation of ocean processes within the ocean model component, or from the ocean-atmosphere interface and the cold land temperature bias could arise from a poor representation of land processes in the land model component. However, as all these components are coupled and interactive it very difficult to identify which component is causing the bias. Most of the models exhibit a strong ENSO-monsoon teleconnection compared with the observations, and only a few models failed to portray the salient features of the ENSO-monsoon teleconnection. The three important aspects of the South Asian monsoon, namely: 1) the mean, 2) the variability and 3) the global teleconnections, seem to be reasonably simulated in most models. However, for a reliable future climate change projection the models need to be improved in the representation of the above salient features over the South Asian summer monsoon region.

REFERENCES

Adler, R.F., Huffman, G.J., Chang, A., Ferraro, R., Xie, P., Janowiak, J., Rudolf, B., Schneider, U., Curtis, S., Bolvin, D., Gruber, A., Susskind, J., Arkin, P., Nelkin, E. (2003) The Version 2 Global Precipitation Climatology Project (GPCP), Monthly Precipitation Analysis (1979-Present). J Hydrometeor 4: 1147-1167

Ailikun, B., Yasunari, T. (2001) ENSO and Asian summer monsoon: persistence and transitivity in the seasonal march. J Meteor Soc Jap 79: 145–159

Annamalai, H., Hamilton, K., Sperber, K.R. (2007) South Asian summer monsoon and its relationship with ENSO in the IPCC AR4 simulations. J Clim 20:1071–1092

Bollasina, M., Nigam, S. (2008) Indian Ocean SST, evaporation, and precipitation during the South Asian summer monsoon in IPCC-AR4 coupled simulations. Clim Dyn 33:1017–1033

Chang, C.P., Harr, P., Ju, J. (2001) Possible roles of Atlantic circulations on the weakening Indian monsoon rainfall-ENSO relationship. J Clim 14: 2376–2380

Christensen, J.H., Hewitson, B., Busuioc, A., Chen, A., Gao, X., Held, I., Jones, R., Kolli, R.K., Kwon, W.T., Laprise, R., Magaña Rueda, V., Mearns, L., Menendez, C.G., Raisanen, J., Rinke, A., Sarr, A., Whetton, P. (2007) Regional Climate Projections Climate Change 2007: The Physical Science Basis Contribution of Working Group I to the Fourth Assessment Report of the Intergovernmental Panel on Climate Change. In: S Solomon, Qin D, Manning M, Chen Z, Marquis M, Averyt KB, Tignor M, Miller HL (eds). Cambridge University Press, Cambridge United Kingdom and New York, NY, USA, 996p

Compo, G.P., & Coauthors (2011) The Twentieth Century Reanalysis Project. Quarterly J. Roy. Meteorol. Soc., 137, 1-28

Covey, C., AchutaRao K.M., Cubasch, U., Jones, P., Lambert, S.J., Mann, M.E., Phillips, T.J., Taylor, K.E. (2003) An overview of results from the Coupled Model Intercomparison Project. Glob Planet Change 37: 103–133

IPCC (1996) Climate Change 1995: The Science of Climate Change Contribution of Working Group I to the Second Assessment Report of the Intergovernmental Panel on Climate Change. In: Houghton, J.J., MeiroFilho, L.G., Callander, B.A., Harris, N., Kattenberg, A., Maskell, K. (eds). Cambridge University Press, Cambridge United Kingdom and New York, NY, USA, 572 pp

IPCC (2001) Climate Change 2001: The Scientific Basis Contribution of Working Group I to the Third Assessment Report of the Intergovernmental Panel on Climate Change. In: Houghton, J.T., Ding, Y., Griggs, D.J., Noguer, M., VanderLinden, P.J., Dai, X., Maskell, K., Johnson, C.A. (eds). Cambridge University Press, Cambridge United Kingdom and New York, NY, USA, 881 pp

IPCC (2007) Climate Change 2007: The Physical Science Basis Contribution of Working Group I to the Fourth Assessment Report of the Intergovernmental Panel on Climate Change. In: S. Solomon, Qin, D., Manning, M., Chen, Z., Marquis, M., Averyt, K.B., Tignor, M., Miller, H.L. (eds). Cambridge University Press, Cambridge United Kingdom and New York, NY, USA, 996p

Kang, I.S., Jin, K., Wang, B., Lau, K.M., Shukla, J., Krishnamurthy, V., Schubert, S.D., Waliser, D.E., Stern, W.F., Kitoh, A., Meehl, G.A., Kanamitsu, M., Galin, V.Y., Satyan, V., Park, C.K., Liu, Y.

(2002) Intercomparison of the climatological variations of Asian summer monsoon precipitation simulated by 10 GCMs. Clim Dyn 19: 383–395

Kang, I.S., Lee, J.Y., Park, C.K. (2004) Potential predictability of summer mean precipitation in a dynamical seasonal prediction system with systematic error correction. J Clim 17:834–844

Kawamura, R., Uemura, K., Suppiah, R. (2005) On the recent change of the Indian summer monsoon-ENSO relationship. SOLA 1: 201–204

Kripalani, R.H., Oh, J.H., Kulkarni, A., Sabade, S.S., Chaudhari, H.S. (2007) South Asian summer monsoon precipitation variability: Coupled climate model simulations and projections under IPCC AR4. Theor Appl Climatol 90:133–159

Krishna Kumar, K., Rajagopalan, B., Cane, M.A. (1999) On the weakening relationship between the Indian monsoon and ENSO. Science 284:2156–2159

Lin, J.L. (2007) The double-ITCZ problem in IPCC AR4 coupled GCMs: ocean-atmosphere feedback analysis. J Clim 20:4497– 4525

Meehl, G.A., Covey, C., McAvaney, B., Latif, M., Stouffer, R.J. (2005) Overview of the coupled model intercomparison project. Bull Am Met Soc 86:89–93

Parthasarathy, B., Munot, A.A., Kothwalae, D.R. (1994) All India monthly and seasonal rainfall series – 1871–1993. Theor Appl Climatol 49: 217–224.

Pant, G.B., Parthasarathy, B. (1981) Some aspects of an association between the southern oscillation and Indian summer monsoon. Arc Met Geophy Biok l B 29(2):245–252.

Pant, G.B., Rupa Kumar, K. (1997) Climate of South Asia. Wiley, New York, pp 176–179

Prasanna, V., Yasunari, T. (2011) Simulated Changes in the atmospheric water balance over south Asia in the eight IPCC-AR4 coupled climate models. Theor App Clim 104:139-158.

Preethi, B., Kripalani, R.H., Krishna Kumar, K. (2010) Indian summer monsoon rainfall variability in global coupled ocean-atmospheric models. Cli Dyn, DOI 10.1007/s00382-009-0657, 35:1521-1539.

Rajeevan, M., Unnikrishnan, C.K., Preethi, B. (2011) Evaluation of the ENSEMBLES multi-model seasonal forecasts of the Indian Summer Monsoon Variability. Cli Dyn, DOI 10.1007/s00382-011-1061.

Rasmusson, E.M., Carpenter, T.H. (1983) The relationship between eastern equatorial Pacific sea surface temperatures and rainfall over India and Sri Lanka. Mon Wea Rev 111:517–528

Rayner, N.A., Parker, D.E., Horton, E.B., Folland, C.K., Alexander, L.V., Rowell, D.P., Kent, E.C., Kaplan, A. (2003) Global analyses of sea surface temperature, sea ice, and night marine air temperature since the late nineteenth century J. Geophys. Res.Vol. 108, No. D14, 4407

Rupakumar, K., Krishna Kumar, K., Prasanna, V., Kamala, K., Deshpande, N.R., Patwardhan, S.K., Pant, G.B. (2003) Future Climate Scenarios. In: Climate Change and India: Vulnerability Assessment and Adaptation, Universities Press (India) Pvt Ltd, Hyderabad, pps: 69-127

Ueda, H., Iwai, A., Kuwako, K., Hori, M.E. (2006) Impact of anthropogenic forcing on the Asian summer monsoon as simulated by 8 GCMs. Geophys Res Lett 33: doi: 101029/2005GL025336

Waliser, D.E., Jin, K., Kang, I.S., Stern, W.F., Schubert, S.D., Wu, M.L.C., Lau, K.M., Lee, M.I., Krishnamurthy, V., Kitoh, A., Meehl, G.A., Galin, V.Y., Satyan, V., Mandke, S.K., Wu, G., Liu, Y., Park, C.K. (2003) AGCM simulations of intra-seasonal variability associated with the Asian summer monsoon. Cli Dyn 21: 423–446

Waliser, D., Seo, K.W., Schubert, S., Njoku, E. (2007) Global water cycle agreement in the climate models assessed in the IPCC AR4. Geophys Res Lett 34:L16705

Wang, B., Kang, I.S., Lee, J.Y. (2004) Ensemble simulation of Asian–Australian monsoon variability by 11 AGCMs. J Clim 17: 699–710

Wu, R., Kirtman, B.P. (2007) Regimes of seasonal air–sea interaction and implications for performance of forced simulations. Clim Dyn 29:393–410

Wu, R., Kirtman, B.P., Pegion, K. (2006) Local air-sea relationship in observations and model simulations. J Clim 19:4914–4932

Wu, R., Kirtman, B.P., Pegion, K. (2007) Surface latent heat flux and its relationship with sea surface temperature in the National Centers for Environmental Prediction Climate Forecast System simulations and retrospective forecasts. Geophys Res Lett 34:L17712

Yasunari, T. (1990) Impact of Indian monsoon on the coupled atmosphere/ocean systems in the tropical Pacific. Meteor Atmos Phys 44: 29–41

Acknowledgments

The author would like to acknowledge the Director of the APEC Climate Center (APCC), South Korea for providing the facilities in which to carry out this work. The author would also like to thank the many modeling centers for providing the model simulation for the period of approximately 150 years, and acknowledges CMIP5 for the archiving and provision of large datasets through their website (http://www-pcmdi.llnl.gov/). The diagrams used for this study have been prepared using free software packages such as GrADS, XMGRACE and Intel Fortran and the computational work has been carried out using the Cent-OS operating system environment.

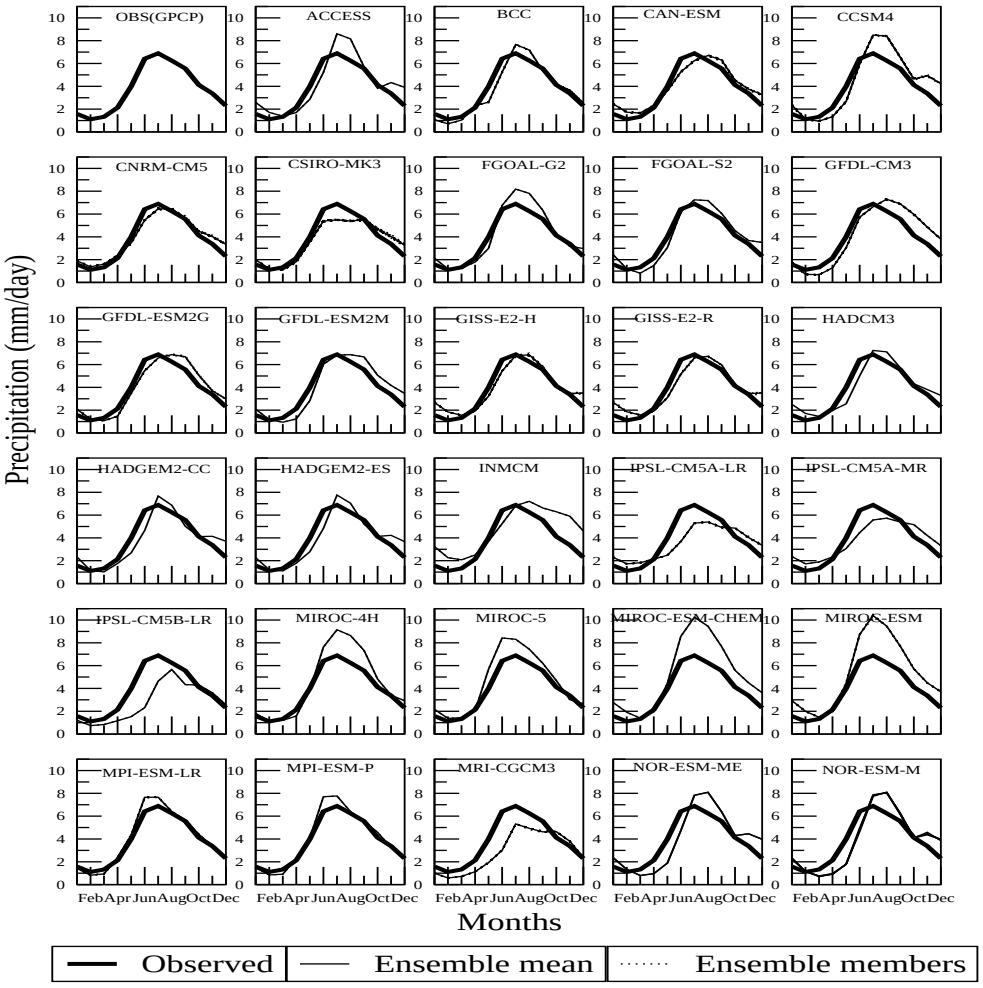

Figure 1 Observed and simulated annual cycle of Precipitation (in mm/day) over South Asia averaged over the domain 5°N-35°N and 65°E-95°E.

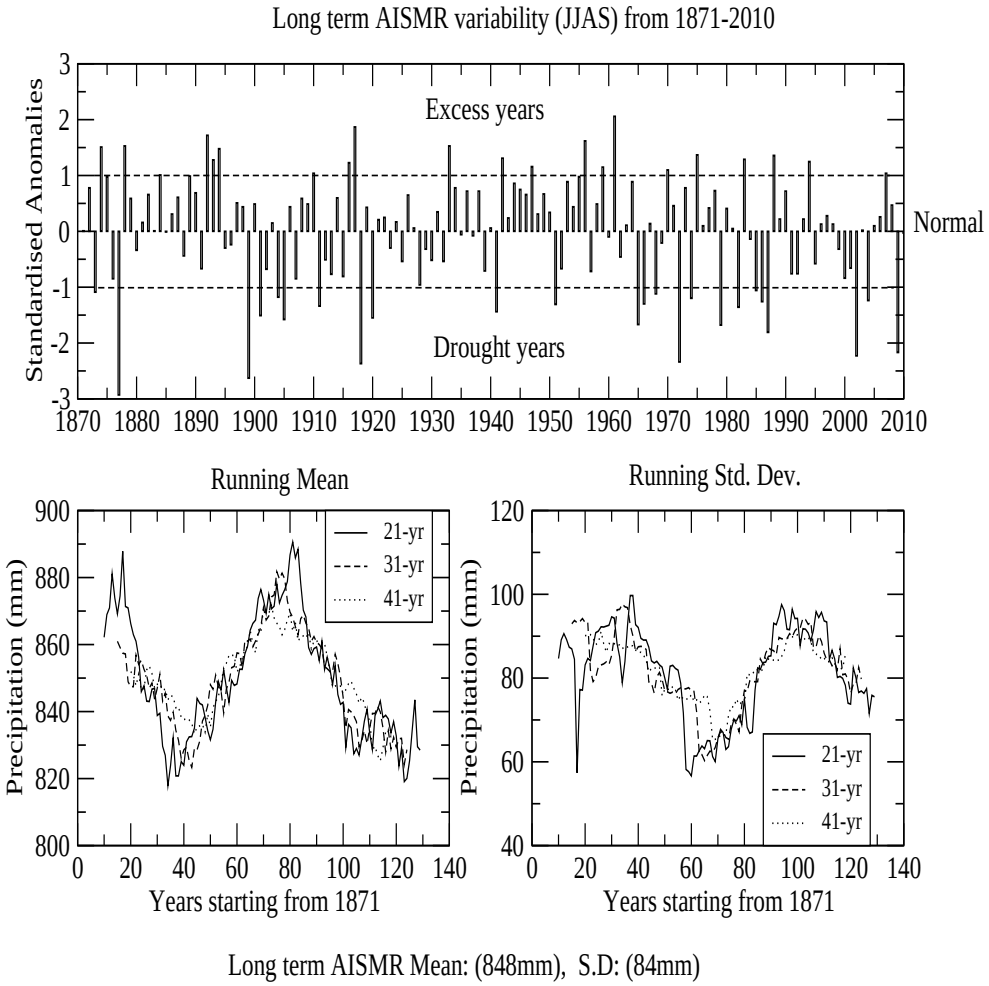

Figure 2 Observed All India Summer Monsoon Rainfall (AISMR) variability for the period 1871–2010, from the Indian Institute of Tropical Meteorology (IITM) monthly time series. a) Standardized anomalies of summer (JJAS) rainfall, b) epochal signature in mean precipitation; and c) epochal signature in precipitation variability.

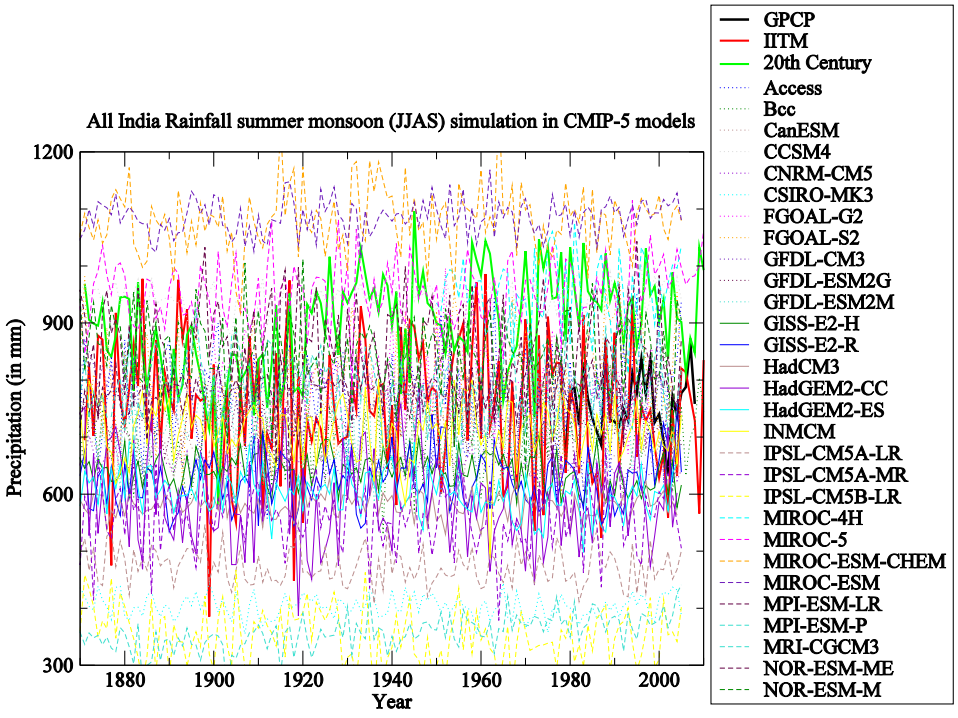

Figure 3 Simulated precipitations for JJAS (in mm/season) in the historical run of CMIP5 coupled climate models.

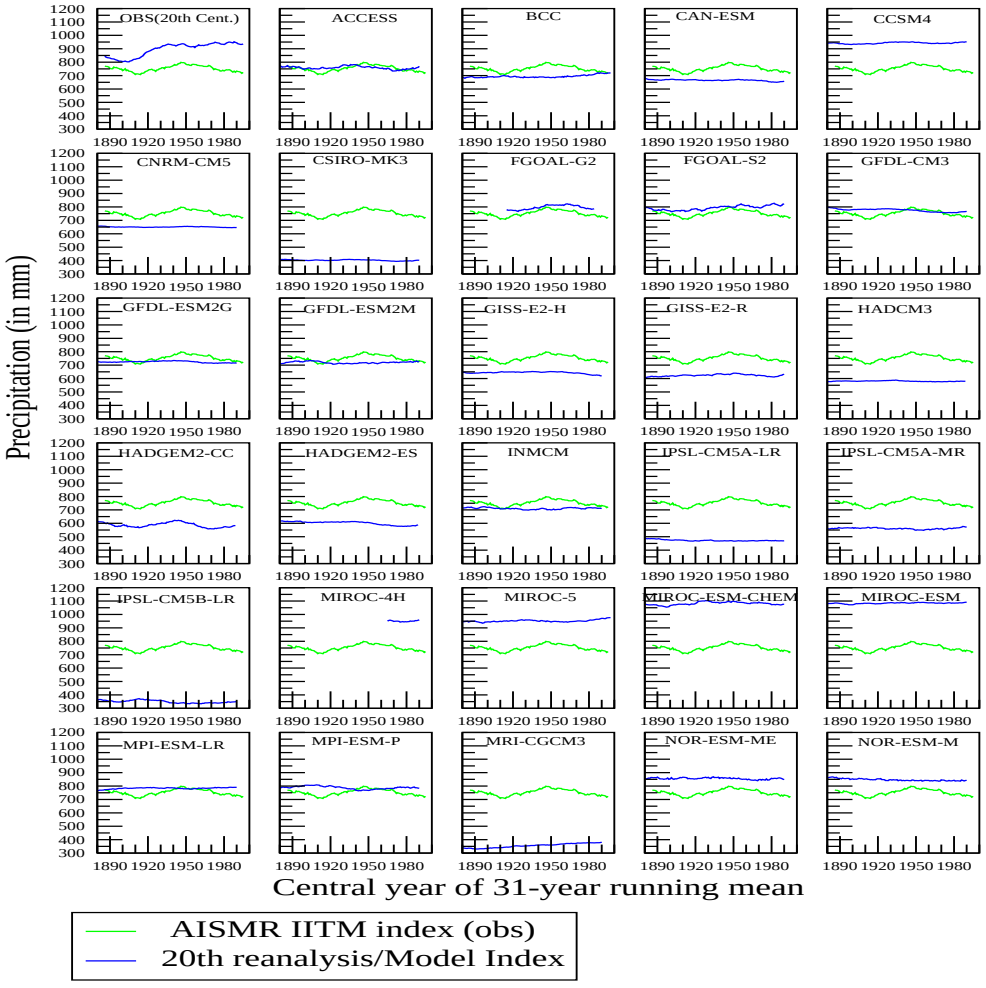

Figure 4 Simulated epochal signature in the mean precipitation for summer (JJAS) from the historical run of CMIP5 coupled climate models (in mm/season). First panel shows the epochal signature in mean precipitation from the observations (IITM AISMR and 20th century reanalysis).

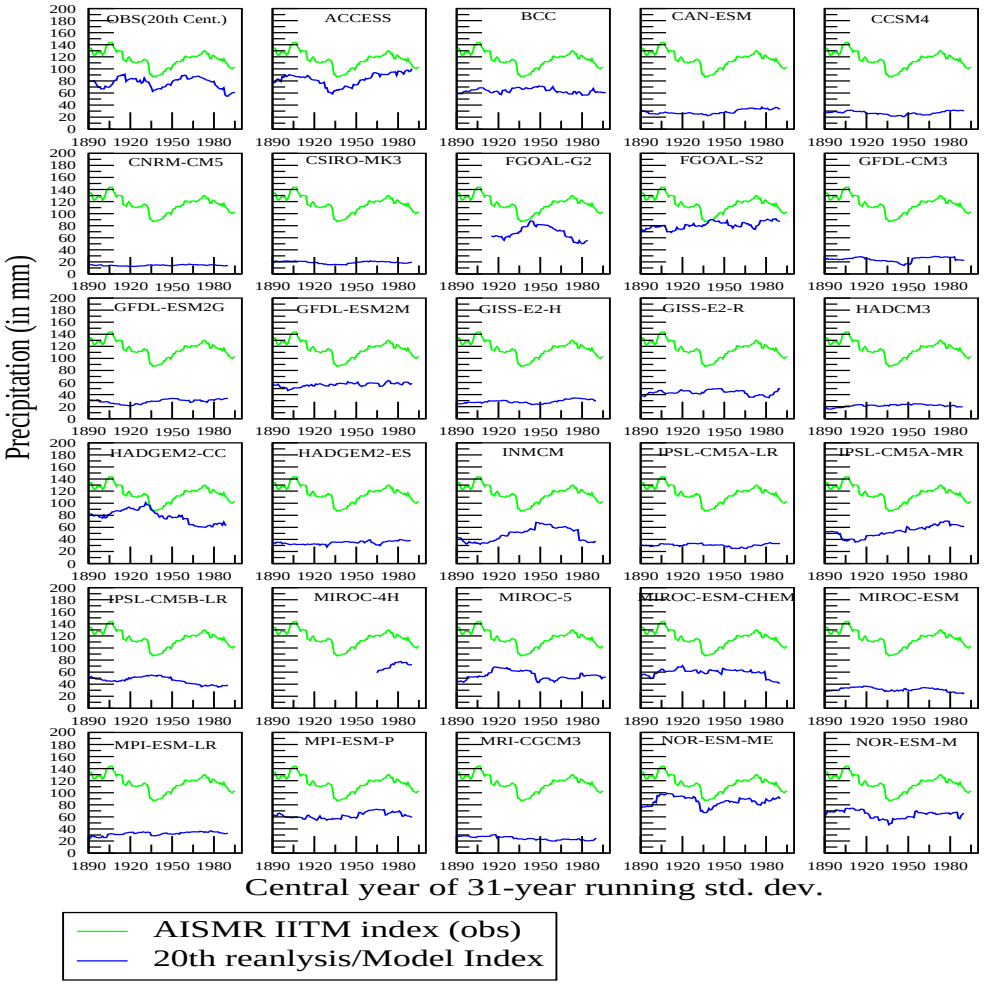

Figure 5 Simulated epochal signature in the precipitation variability for summer (JJAS) from the historical run of CMIP5 coupled climate models (in mm/season). The first panel shows the epochal signature in the precipitation variability from the observations (IITM AISMR and 20th century reanalysis).

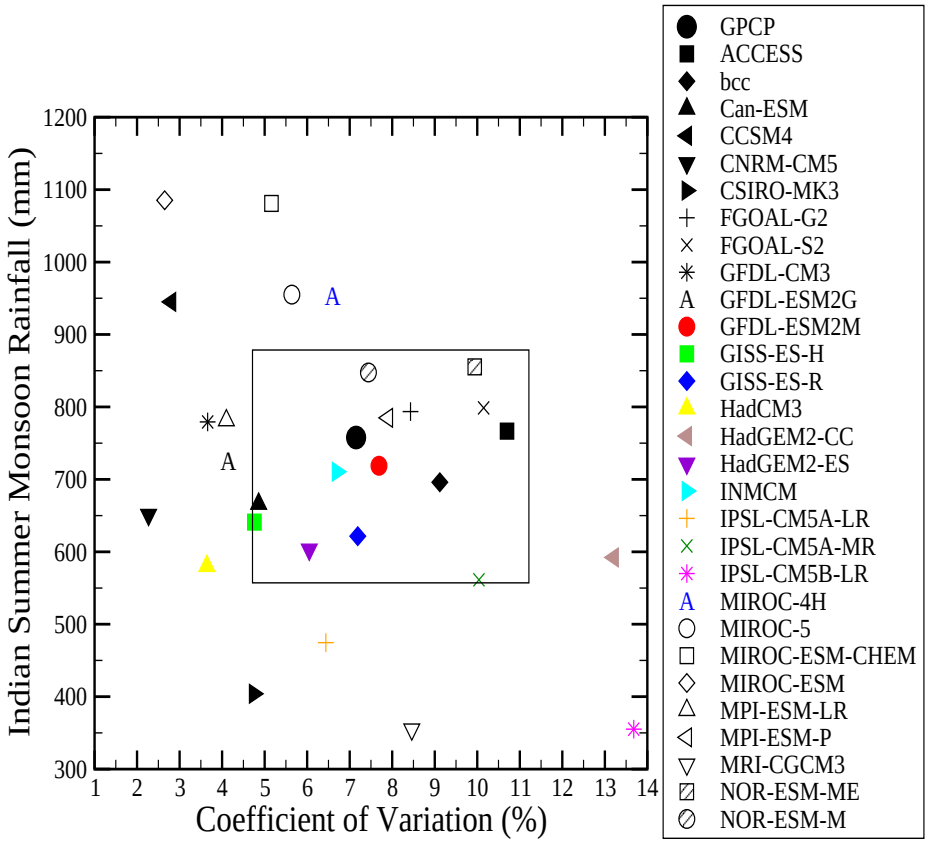

Figure 6 Scatter plot of ISMR (mm) and CV (%) from observation (GPCP Rainfall) and CMIP5 coupled climate model simulations over South Asia. Observation is denoted in black. The 29 different models are represented in different colors.

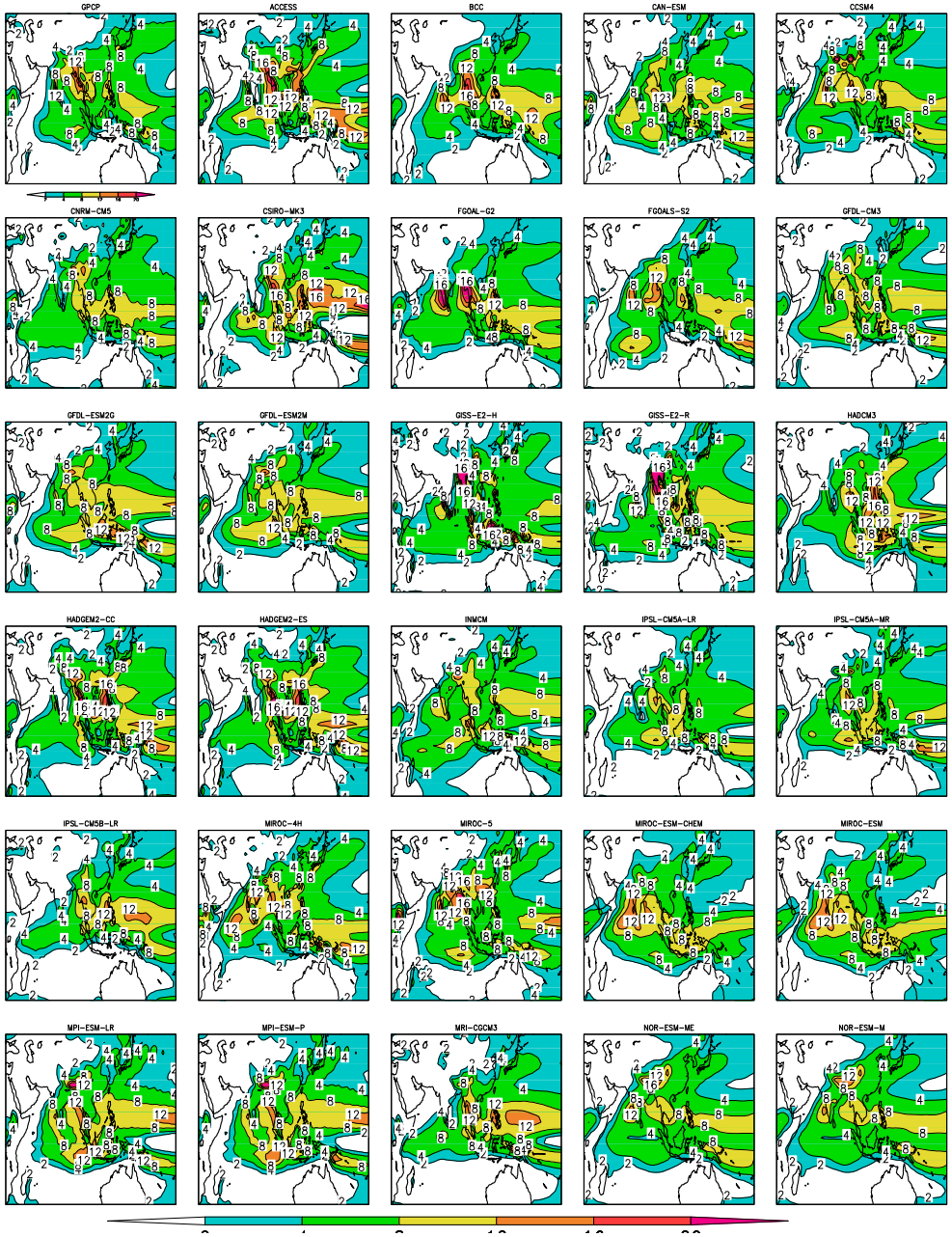

Figure 7 Climatological seasonal mean summer (JJAS) Precipitation, (P) (mm/day), for 29 models in the historical run of CMIP5 coupled climate model simulations over South Asia. The first panel shows the observation (GPCP: 1979–2008).

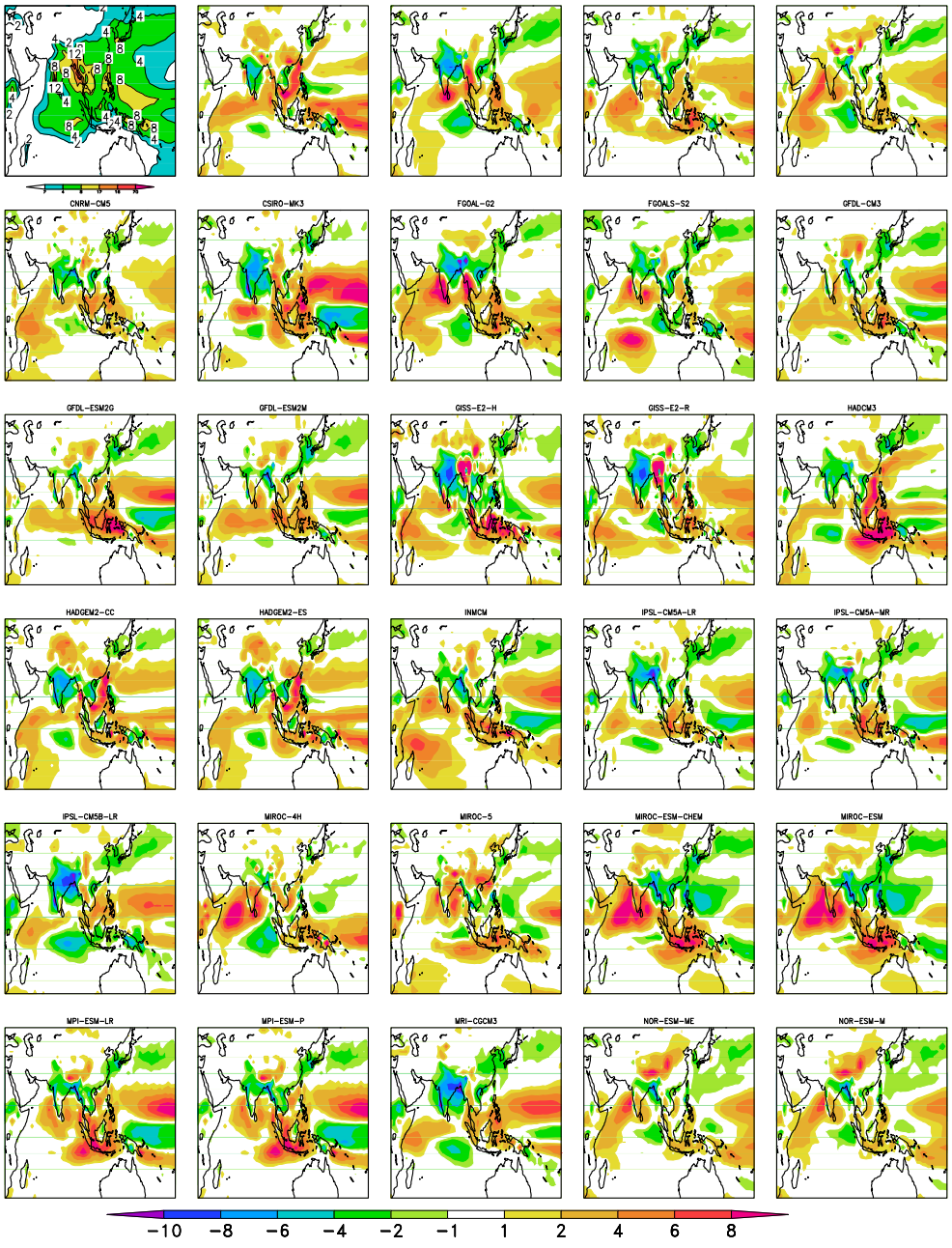

Figure 8 Climatological seasonal mean summer (JJAS) Precipitation bias, (P) (mm/day), for 29 models in the historical run of CMIP5 coupled climate model simulations from observation. First panel shows the climatological seasonal mean summer precipitation from observation (GPCP: 1979–2008).

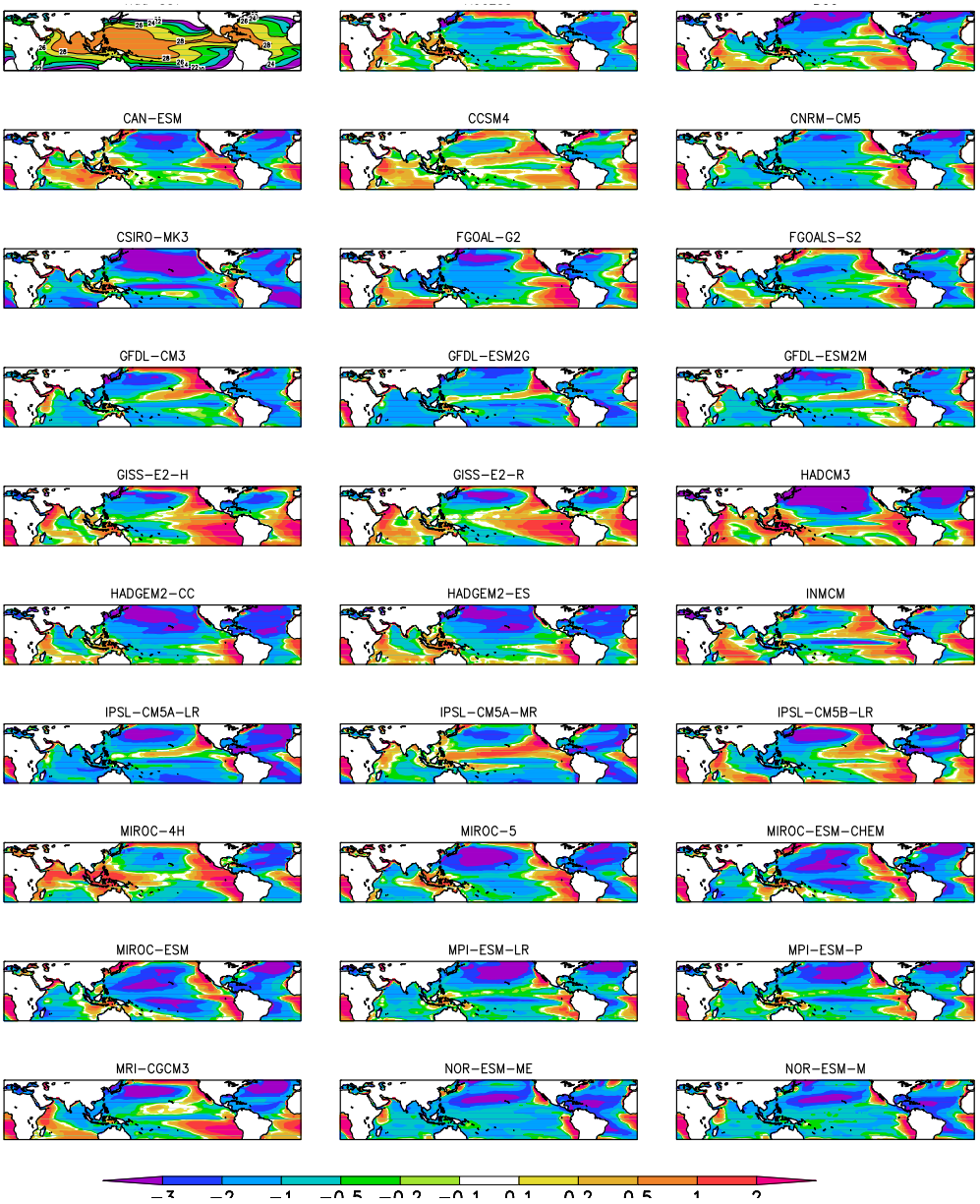

Figure 9 Climatological seasonal mean summer (JJAS) Sea Surface Temperature bias, (SST) (°C), for 29 models in the historical run of CMIP5 coupled climate model simulations from observation. The first panel shows the climatological seasonal mean summer SST from observation (HADISST: 1871–2010).

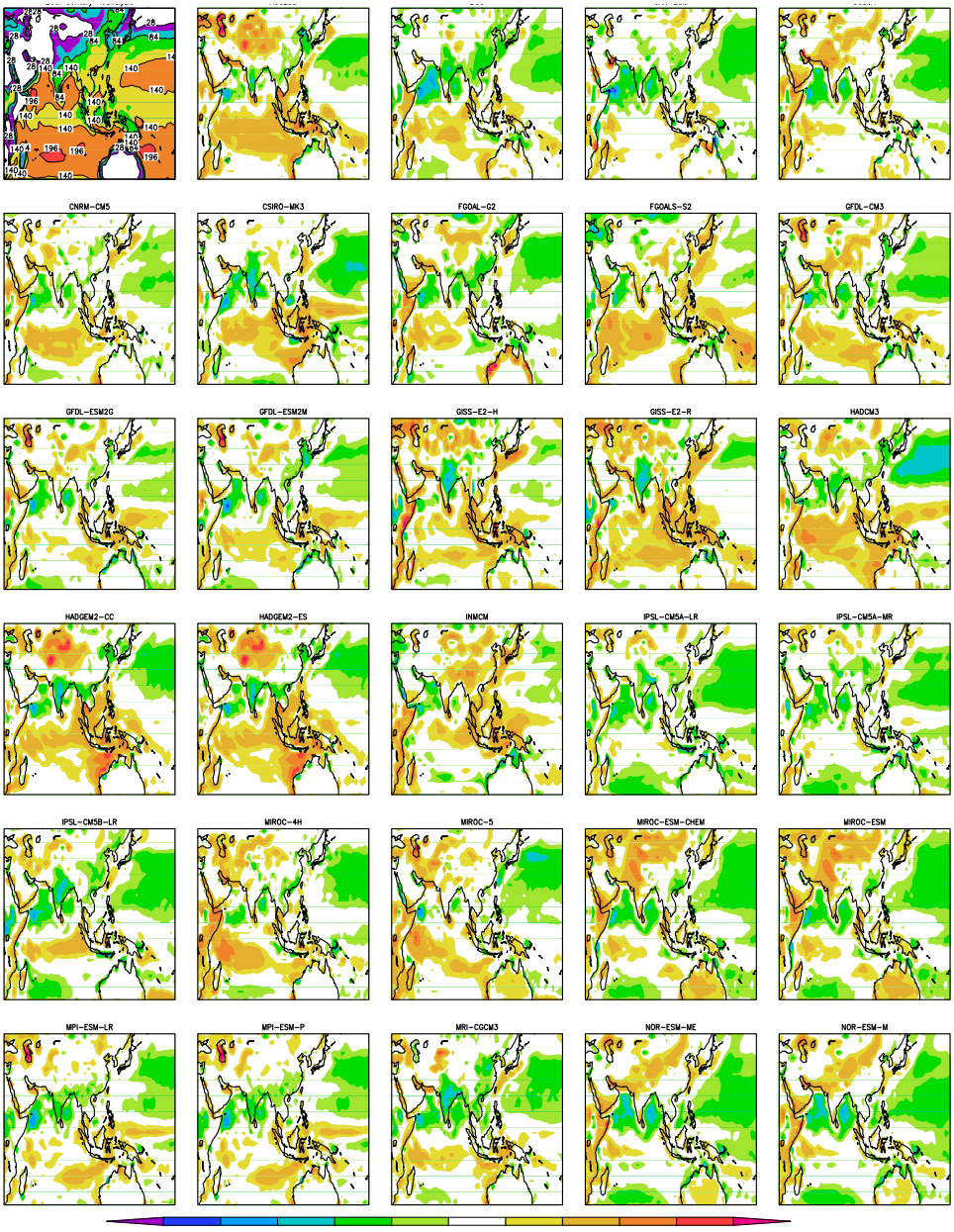

Figure 10 Climatological seasonal mean summer (JJAS) Evaporation bias, (LHF) (Watt m^{-2}), for 29 models in the historical run of CMIP5 coupled climate model simulations from observation. The first panel shows the climatological seasonal mean summer evaporation from observation (20^{th} century reanalysis: 1871–2010).

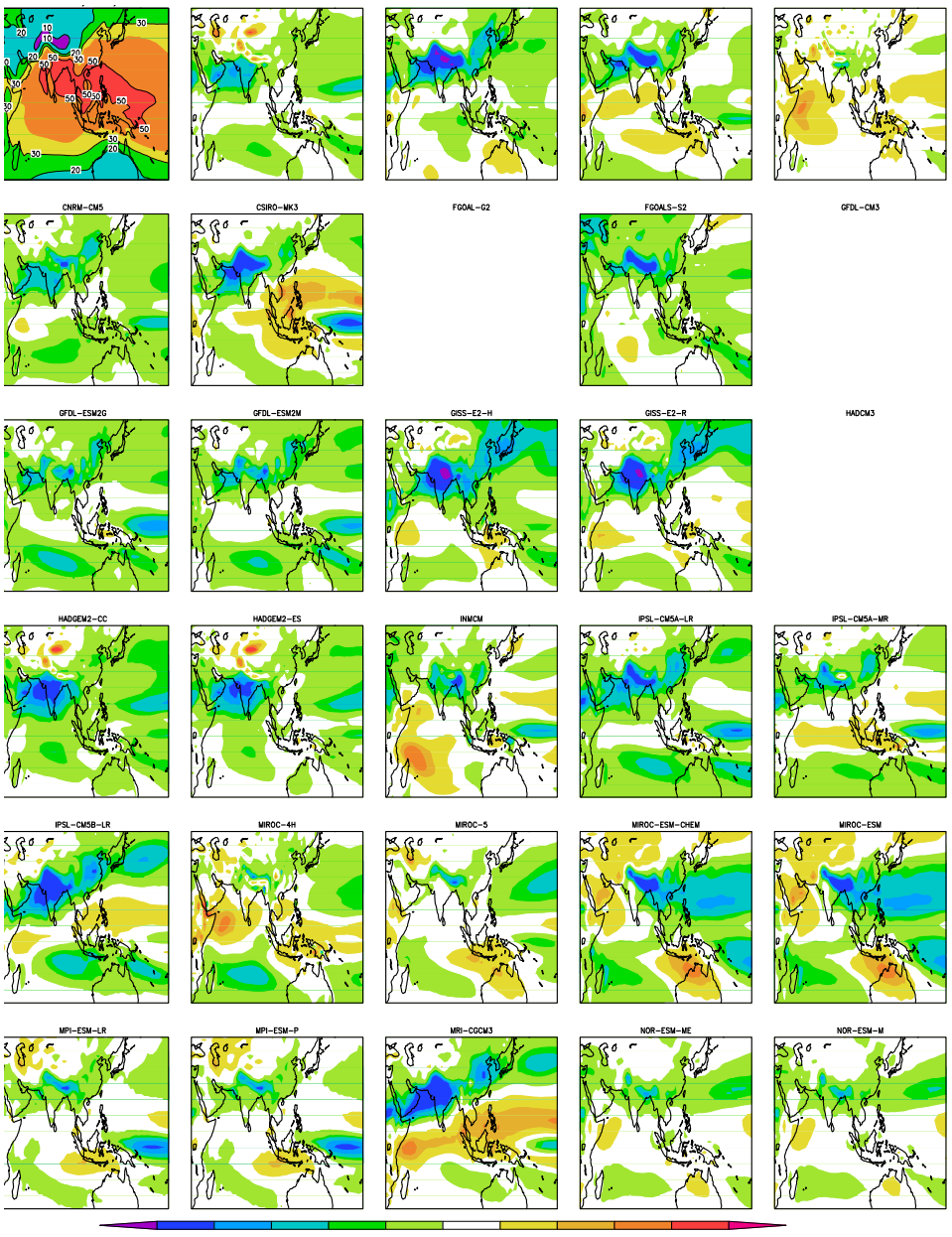

Figure 11 Climatological seasonal mean summer (JJAS) Precipitable water bias, (PRW) (mm), for 29 models in the historical run of CMIP5 coupled climate model simulations from observation. The first panel shows the climatological seasonal mean summer precipitable water from the observation (20th century reanalysis: 1871–2010).

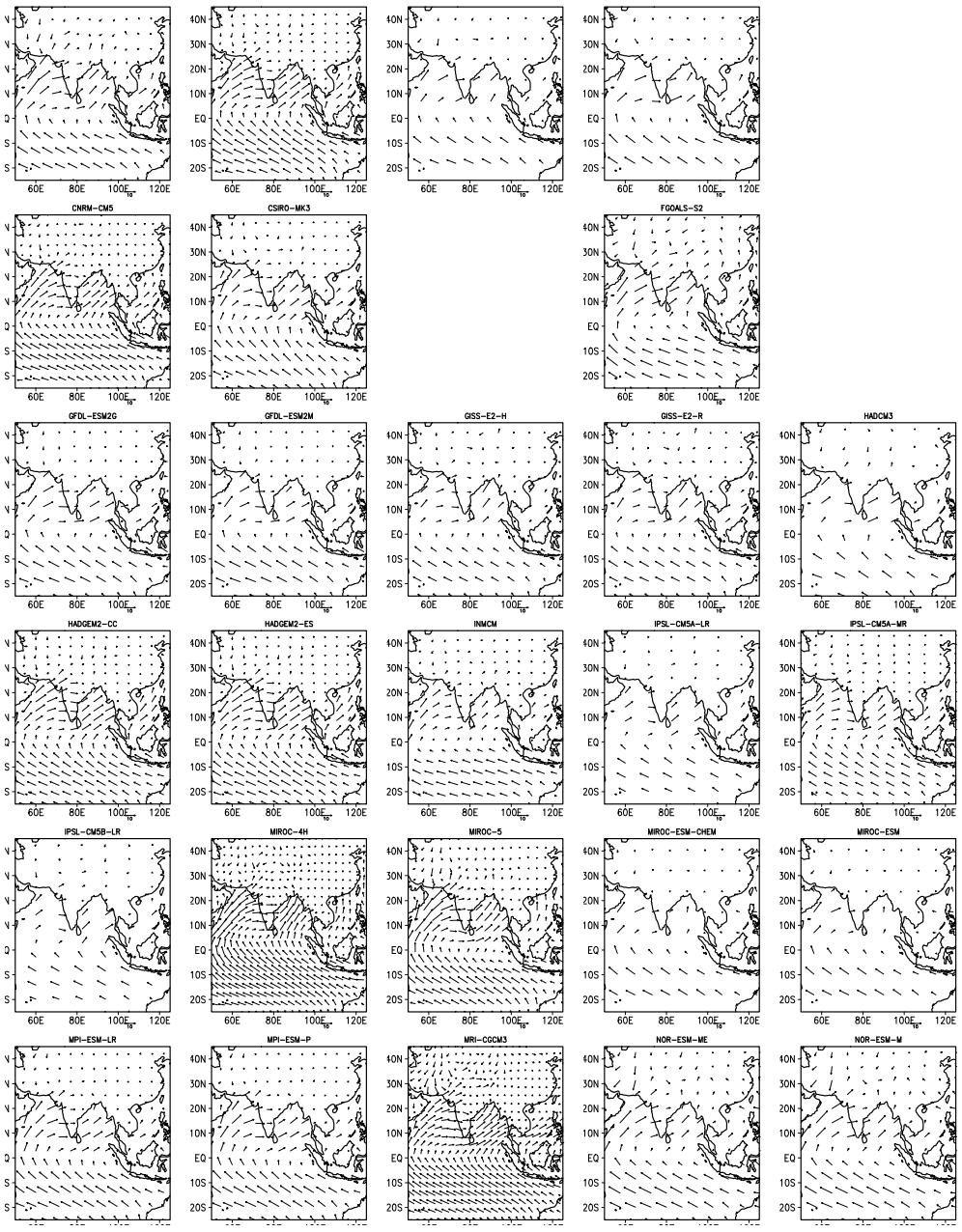

Figure 12 Climatological seasonal mean summer (JJAS) Winds, (U, V) (ms^{-1}), for 29 models in the historical run of CMIP5 coupled climate model simulations over South Asia. The first panel shows the observation (20^{th} century reanalysis: 1871–2010).

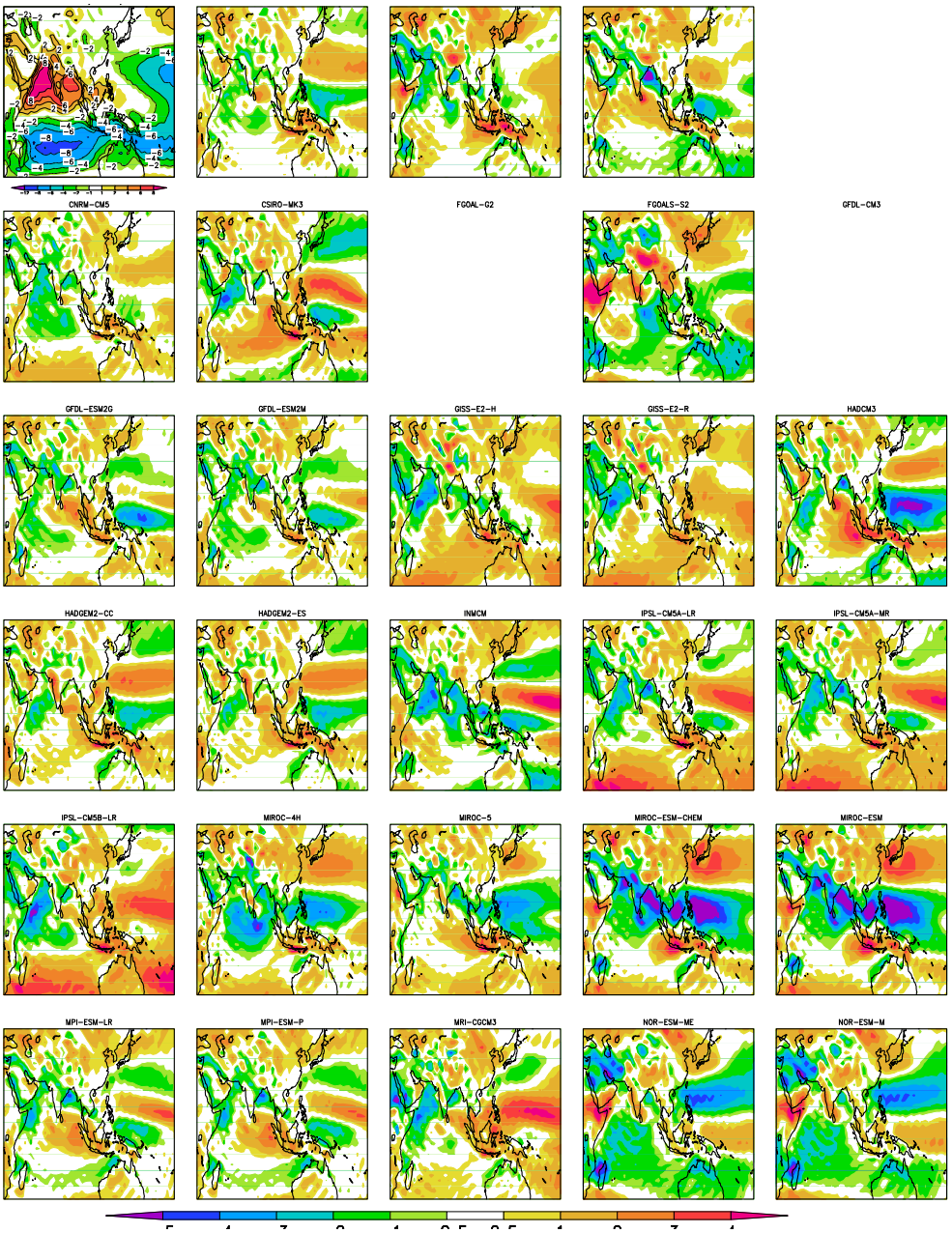

Figure 13 Climatological seasonal mean summer (JJAS) Zonal Wind bias, (U) (ms^{-1}), for 29 models in the historical run of CMIP5 coupled climate model simulations over South Asia. The first panel shows the climatological seasonal mean summer zonal wind from observation (20^{th} century reanalysis: 1871–2010).

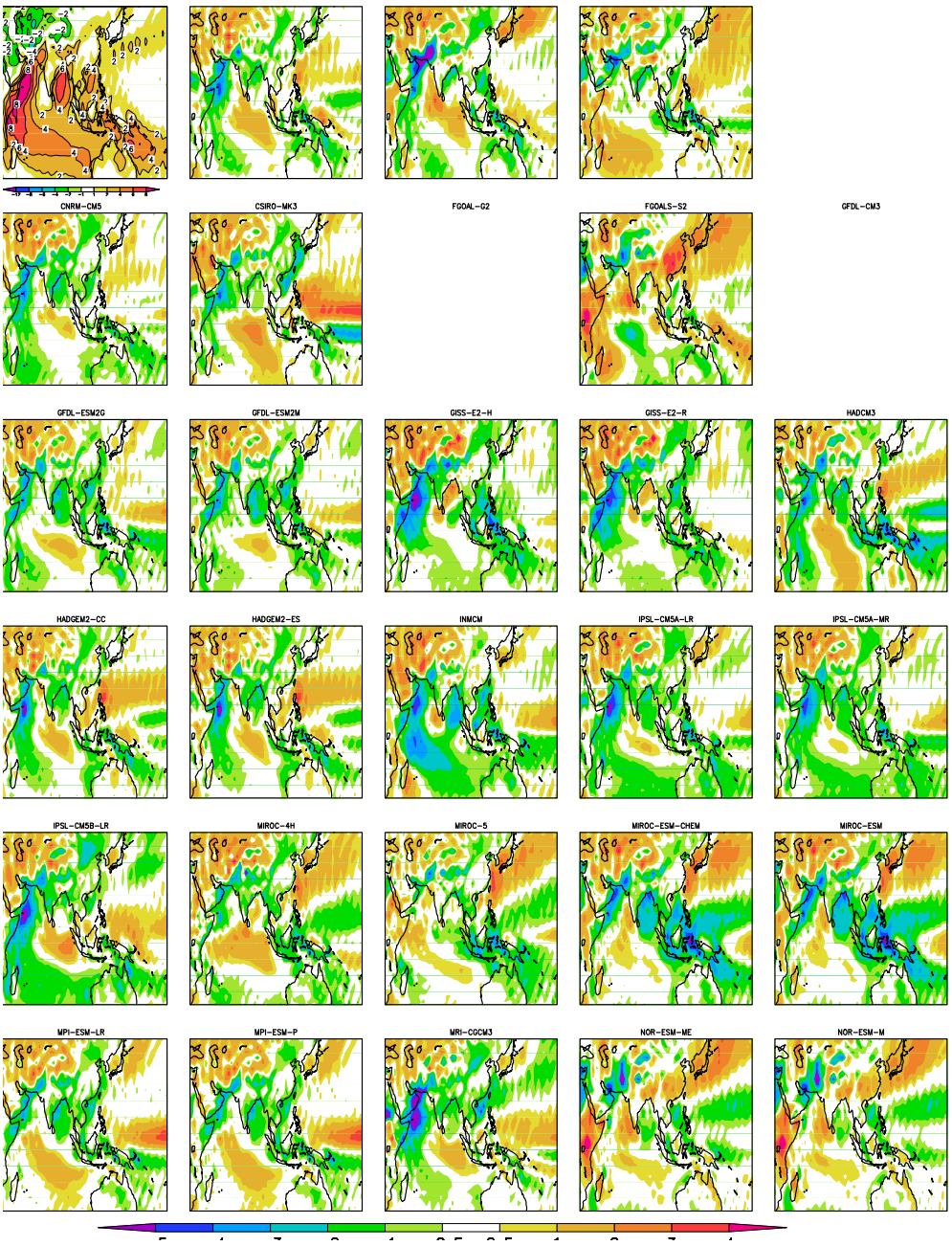

Figure 14 Climatological seasonal mean summer (JJAS) Meridional Wind bias, (U) (ms^{-1}), for 29 models in the historical run of CMIP5 coupled climate model simulations over South Asia. The first panel shows the climatological seasonal mean summer meridional wind from observation (20^{th} century reanalysis: 1871–2010).

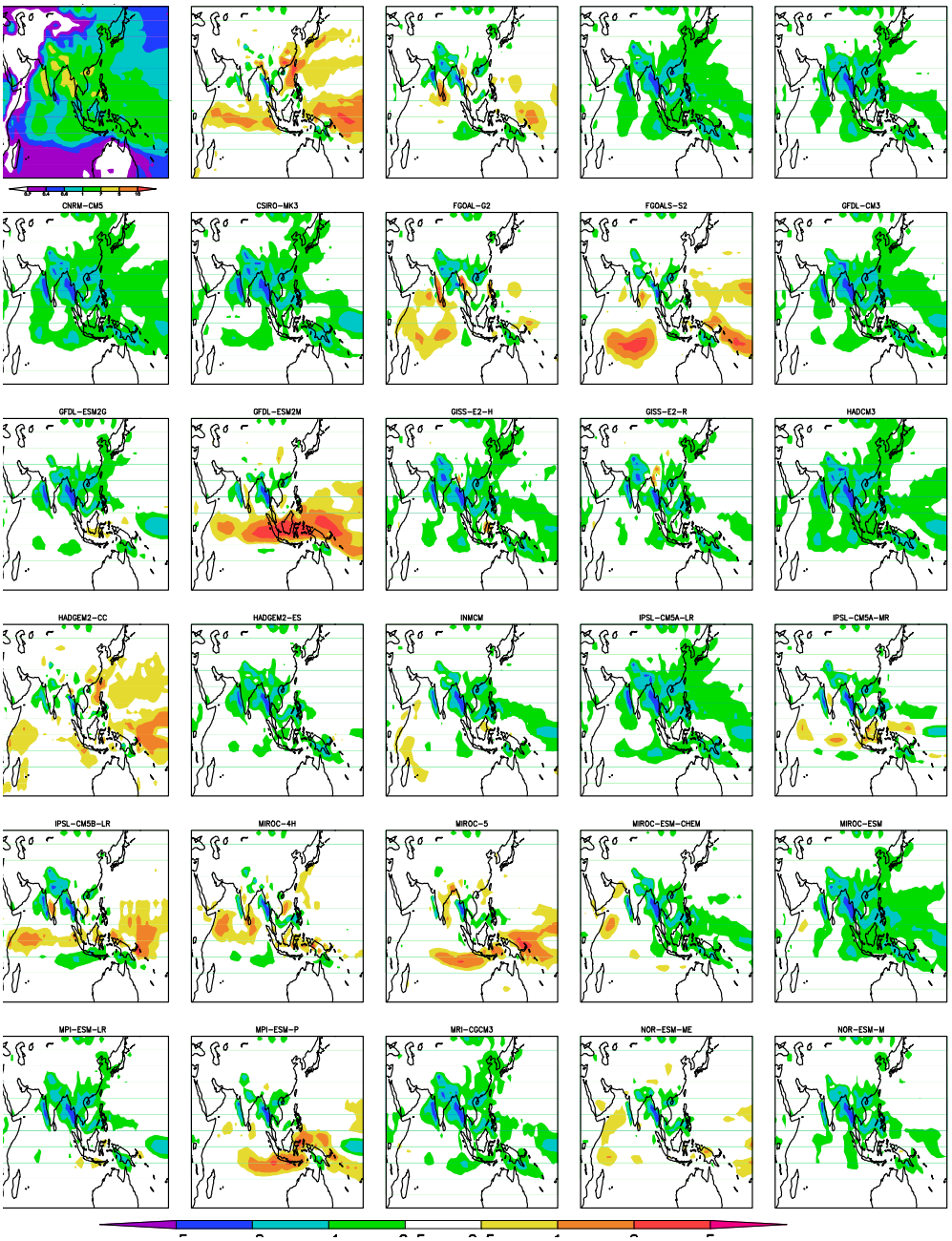

Figure 15 Precipitation variability (JJAS Standard Deviation) bias, (mm/day), for 29 models in the historical run of CMIP5 coupled climate model simulations from observation. The first panel shows JJAS precipitation standard deviation from observation (GPCP: 1979–2008).

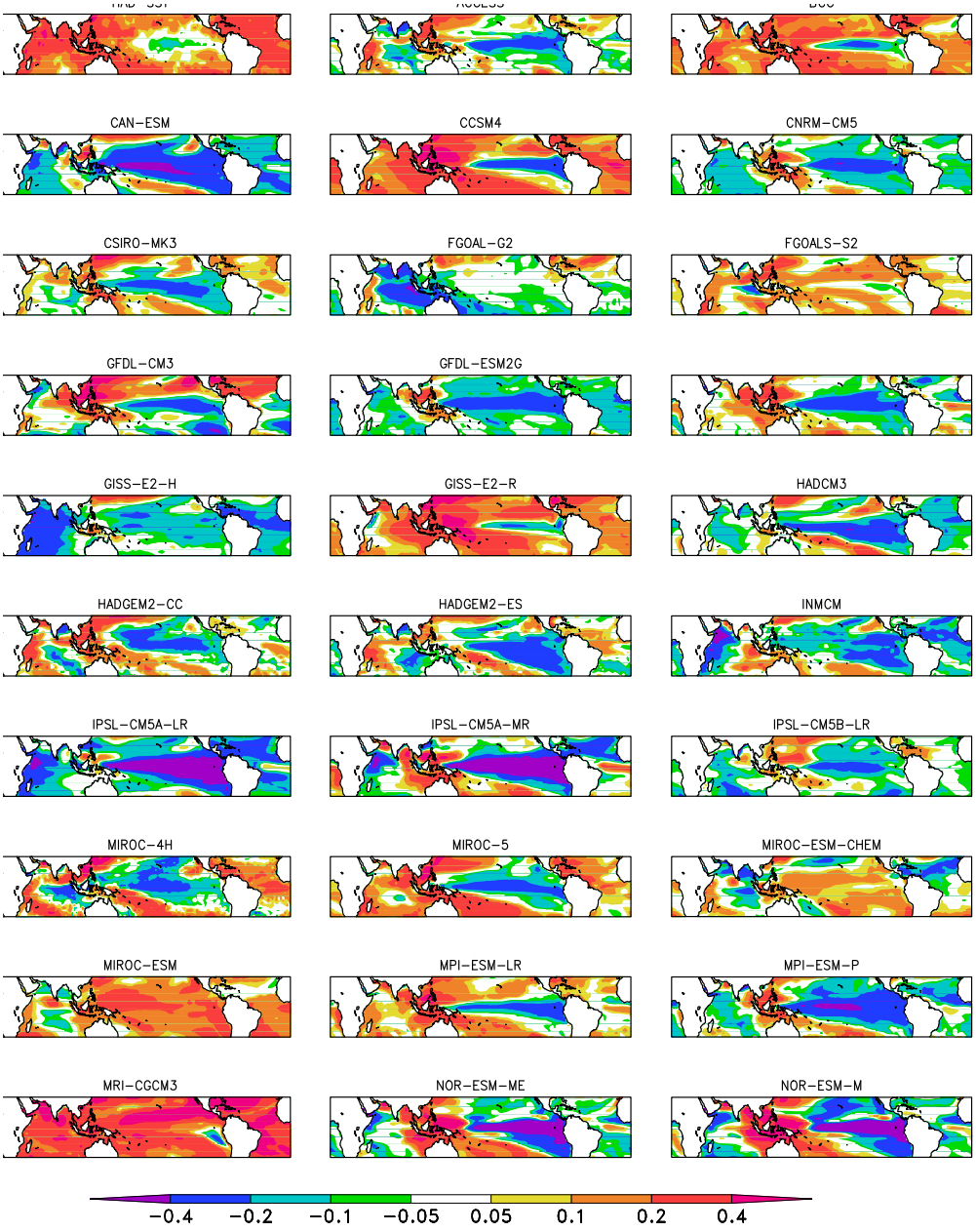

Figure 16 Simultaneous correlation of model Sea Surface Temperature, (SST), with the All Indian Summer monsoon index (AISMR: 5°N-35°N and 65°E-95°E) from 29 models in the historical run of CMIP5 coupled climate model simulations for the summer (JJAS) season. The first panel shows the simultaneous correlation from observation for the summer (JJAS) season. (AISMR: IITM index vs HADISST).

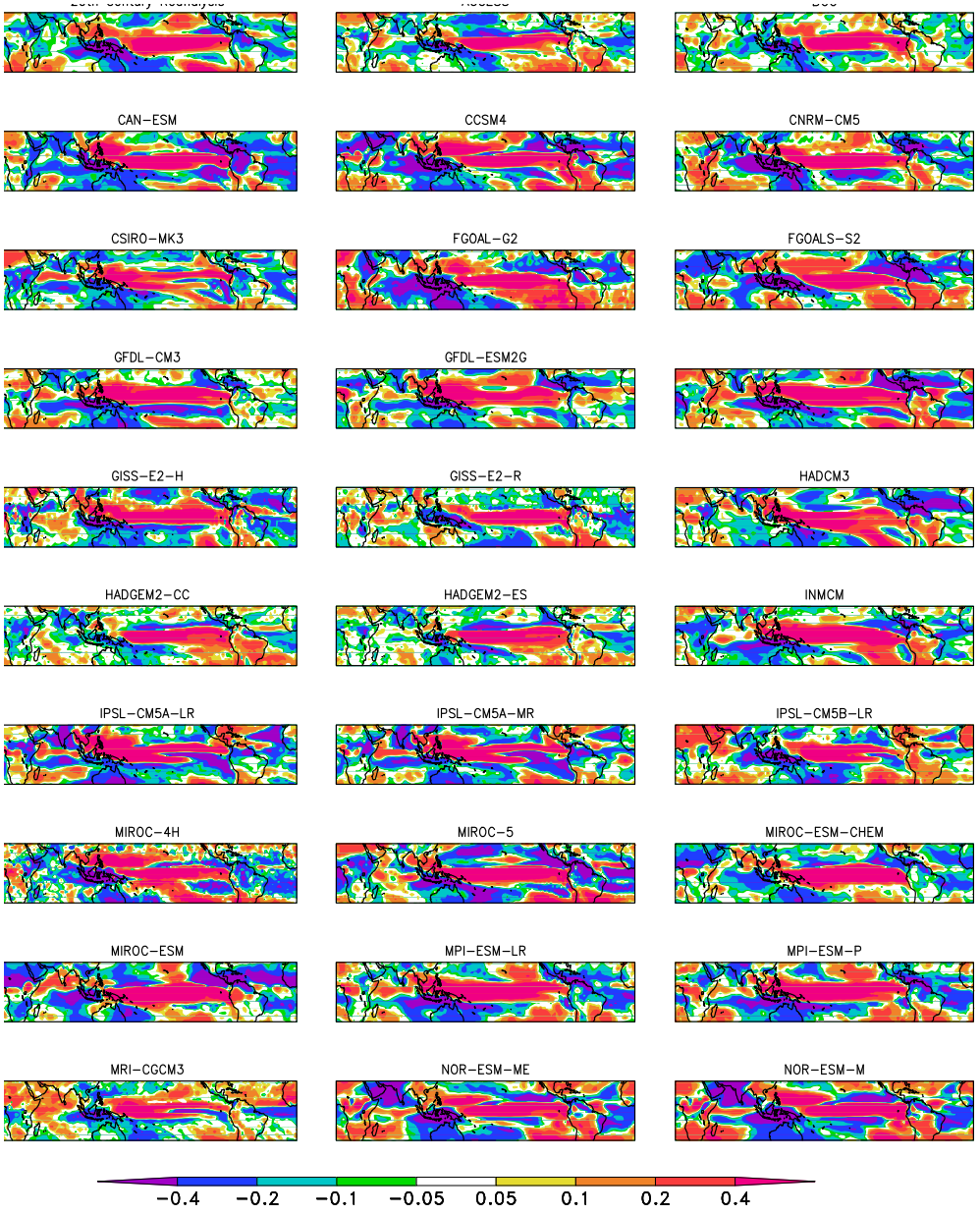

Figure 17 Simultaneous correlation of model precipitation, (P), with the Niño 3.4 index (Niño 3.4: 5°S-5°N and 170°W to 120°W) from 29 models in the historical run of CMIP5 coupled climate model simulations for the summer (JJAS) season. The first panel shows the simultaneous correlation from the observation for the summer (JJAS) season. (Niño 3.4 Index: HADISST vs 20th century reanalysis precipitation).

Table 1 Description of the Twenty nine Coupled Climate Model (CMIP5) Simulations used in the study

No.	Model	Institution	Country	Resolution (Lat x Lon x Time in months)	Time Period	Total no. of years of Simulation	No of ensemble runs
1	ACCESS1-0	CSIRO	Australia	145x192x1872	185001-200512	156	1
2	BCC-CSM1.1	BCC	China	64x128x1956	185001-201212	163	3
3	CanESM2	CCCma	Canada	64x128x1872	185001-200512	156	5
4	CCSM4	NCAR	USA	192x288x1872	185001-200512	156	6
5	CNRM-CM5	CNRM and CERFACS	France	128x256x1872	185001-200512	156	9
6	CSIRO-Mk3.6	CSIRO	Australia	96x192x1872	185001-200512	156	10
7	GFDL-CM3	NOAA GFDL	USA	90x144x1752	186001-200512	146	5
8	GFDL-ESM2G	NOAA GFDL	USA	90x144x1740	186101-200512	145	3
9	GFDL-ESM2M	NOAA GFDL	USA	90x144x1740	186101-200512	145	1
10	GISS-E2-H	NASA/GISS	USA	90x144x1872	185001-200512	156	6
11	GISS-E2-R	NASA/GISS	USA	90x144x1872	185001-200512	156	3
12	HadCM3	MOHC	UK	73x96x1740	186101-200512	145	10
13	HadGEM2-CC	MOHC	UK	145x192x1740	186101-200512	145	1
14	HadGEM2-ES	MOHC	UK	145x192x1740	186101-200512	145	4
15	INM-CM4	INM	Russia	120x180x1872	185001-200512	156	1
16	IPSL-CM5A-LR	IPSL	France	96x96x1872	185001-200512	156	4
17	IPSL-CM5A-MR	IPSL	France	143x144x1872	185001-200512	156	1
18	IPSL-CM5B-LR	IPSL	France	96x96x1872	185001-200512	156	1
19	MIROC-ESM	JAMSTEC, AORI, NIES	Japan	64x128x1872	185001-200512	156	3
20	MIROC-ESM-CHEM	JAMSTEC, AORI, NIES	Japan	64x128x1872	185001-200512	156	1
21	MIROC4h	AORI	Japan	320x640x672	195001-200512	56	1
22	MIROC5	AORI	Japan	128x256x1956	185001-201212	163	1
23	MPI-ESM-LR	MPI-M	Germany	96x192x1872	185001-200512	156	3
24	MPI-ESM-P	MPI-M	Germany	96x192x1872	185001-200512	156	1
25	MRI-CGCM3	MRI	Japan	160x320x1872	185001-200512	156	5
26	NorESM1-M	NCC	Norway	96x144x1872	185001-200512	156	1
27	NorESM1-ME	NCC	Norway	96x144x1872	185001-200512	145	3
28	FGOAL-g2	FGOAL	China	60x128x1200	190001-199912	100	1
29	FGOAL-s2	FGOAL	China	108x128x1872	185001-200512	156	4

REGIONAL CLIMATE CHANGE SCENARIOS OVER SOUTH ASIA IN CMIP5 COUPLED CLIMATE MODEL SIMULATIONS

ABSTRACT

This paper evaluates the performance of a suite of state-of-the-art coupled atmosphere-ocean general circulation models (AOGCMs) in their representation of regional characteristics of the hydrological cycle and temperature over South Asia. The temperature and hydrological cycle are presented here, based on AOGCM experiments conducted for two types of future greenhouse gas emission scenarios (RCP4.5 and RCP8.5) extending up to the end of 21st century. Despite having a relatively coarse resolution, the AOGCMs have shown a reasonable skill in depicting the hydrological cycle over the South Asian region, but there are considerable biases in their depiction, with inter-model differences. The regional climate change scenarios of temperature (T), atmospheric water balance components, precipitation, moisture convergence and evaporation (P, C and E) up to the end of the 21st century based on CMIP5 modeling experiments conducted for (RCP4.5 and RCP8.5), indicate a marked increase in both rainfall and temperature within the 21st century, becoming particularly conspicuous after the 2050's. The monsoon rainfall and atmospheric water balance changes under both the RCP4.5 and RCP8.5 scenarios are discussed in detail in this paper, and spatial patterns of rainfall change projections indicate a maximum increase over South Asia in most of the models. Model simulations under scenarios of increased greenhouse gas concentrations suggest that the intensification of the hydrological cycle is driven mainly by an increased moisture convergence due to the increase in the water holding capacity of the atmosphere in a warmer environment. The intensification of the hydrological cycle is greater for RCP8.5 compared with RCP4.5, and a few of the models indicate an increased variance of temperature and rainfall in a warmer environment. While the scenarios presented in this study are indicative of the expected range of rainfall and water balance changes, it must be noted that the quantitative estimates still have large uncertainties associated with them.

1. INTRODUCTION

A series of Intergovernmental Panel on Climate Change (IPCC) reports note that the current version of atmosphere-ocean general circulation models (AOGCMs) have made general improvements in their capability of simulating the observed features of the present-day climate on a large and continental scale (IPCC, 1996, 2001, 2007; Christensen *et al.* 2007). Though it is a cause for concern that the models produce

large inter-model differences on a regional scale with consequent uncertainties, it is encouraging that the AOGCMs have shown significant and rapid improvement over the past couple of decades in their ability to capture the gross observed climate features. The effects of climate change are expected to be greatest in the developing world, especially in countries reliant on primary production as a major source of income. Further research is therefore required to strengthen future assessments and reduce uncertainties, in order to ensure that sufficient information is available for policy makers to respond to the possible consequences of climate change; including research in and by developing countries. One of the highest priorities to narrow the gaps between current knowledge and the ability to make effective policies is the need for quantitative assessments based on the sensitivity, adaptive capacity and vulnerability to climate change of developing countries, particularly in terms of major agro-economic indicators. To systematically pursue such assessments, the most fundamental requirement is the availability of reliable estimates of future climatic patterns on the regional scale, which can be readily used by different impact assessment groups. This, in turn, requires the systematic validation of climate model simulations and the development of suitable regional climate change scenarios with accurate estimates of the associated uncertainties.

Climate variation and change caused by external forcings may be partly predictable, particularly on the larger (continental and global) spatial scale. Because human activities, which result in the emission of greenhouse gases or land-use change, result in external forcing, it is believed that the large-scale aspects of human-induced climate change are also partly predictable. However, the ability to actually predict these large-scale aspects of human-induced climate change is limited, due to the inability to accurately predict population change, economic change, technological development, and other relevant characteristics of future human activity. In practice, therefore, carefully constructed scenarios involving human behavior need to be relied upon for the determination of climate projections based on such scenarios.

The results of several AOGCM simulations are presented for the South Asian monsoon region to provide an idea of the models' skill in representing the regional hydrological cycle and of their future projections. Datasets used in the study are

from CMIP5 simulations of AOGCMs forced with reconstructed greenhouse gas and aerosol concentrations to represent the present day climate, (historical run), and future concentrations according to the Representative Concentration Pathways (RCP) 4.5 and 8.5 Scenarios. The likely future change in rainfall and the associated hydrological cycle over the South Asian region is presented.

A long period of available reanalysis data spanning 1850–2000 of precipitation (P) and convergence (C) is calculated and used in this study, from the reanalysis evaporative flux (E), (C = P - E). The South Asian monsoon region in the domain of 0N - 30N and 65E -100E is considered in the reanalysis and in each AOGCM. The area averages of precipitation, convergence and evaporation fields are calculated to generate monthly data for the considered periods of the AOGCM simulations. These monthly data are then used to compute the seasonal totals of P, C and E. Taking the years 1850–2000 as the baseline period (historical run), the seasonal quantities are then examined for their likely future changes until the end of the 21st century.

Prasanna and Yasunari (2011) studied the atmospheric hydrological cycle over the South Asian monsoon region and found that the role of evaporation is crucial in the understanding of the interannual variability of precipitation over the region, and that the contribution of evaporation to precipitation is as large as that of convergence over both dry and wet regimes. In this paper, therefore, the contribution of evaporation is considered to be important when considering projections based on AOGCM results.

The structure of this paper is as follows. Section 2 describes the datasets and methodology. Section 3 discusses the observed and simulated hydrological cycle over South Asia and presents a discussion of the simulated hydrological cycle by the AOGCMs over South Asia. Climate change simulation scenarios of the hydrological cycle over South Asia in 12 AOGCMs are also documented. Section 4 presents the main conclusions and discussion.

2. METHODOLOGY

2.1 Datasets and Methodology

The transient climate change simulations of 12 AOGCMs were used in the present study. These simulations were part of the suite of CMIP5 simulations performed for the IPCC-AR5 scientific assessment report. The data have been obtained from the Program for Climate Model Diagnosis and Inter-comparison (PCMDI) at the Lawrence Livermore National Laboratory (LLNL), USA. The main centers of development of the 12 models used in the study are listed in Table 1, along with their acronyms. Technical details of the above AOGCMs, including resolution and various physical parameterization schemes are summarized in the references cited in Table 1. The 12 models were used to simulate global climate representing the present climate (historical run) and the likely future change with RCP4.5 and RCP8.5 forcings.

2.1.1 Model Experiments

The use of scenarios is among the main methods used to address the complexity and uncertainty of future challenges associated with climate change. The IPCC initiated the development of greenhouse-gas emission scenarios designed to serve as inputs to GCMs and facilitate the assessments of climate-change impacts (IPCC, 1996). The simulation experiments used in the present study are as follows:

(i) Historical Run

The historical run is a control integration, in which the atmospheric forcing in terms of the greenhouse gas concentration is taken from a reconstructed time series of concentrations and performed for a period of approximately 150 years; typically from 1850–2005. The climatology constructed is then taken from the 150 years of the historical run to represent the present day climate (1850–2005) in each model.

(ii) RCP 4.5 Scenario

The RCP4.5 scenario falls in the category of a "Medium-High emission scenario". This group of scenarios describes a future world with moderate economic growth.

(iii) RCP 8.5 Scenario

The RCP8.5 scenario falls in the category of a 'High emission scenario'. This group of scenarios describes a future world with extremely rapid economic growth and a global population that peaks in the mid-century and declines thereafter.

Monthly data of precipitation (P), evaporation (E) and temperature (T) from the AOGCMs (Table. 1) are utilized for the three runs. The length of the data used in each of the model runs is: 1800 months for the historical run to correspond with the present climate of 1850–2000 (i.e., 150 yrs of the historical run per model), and 1200 months for RCP4.5 and RCP8.5 (i.e., 100 yrs × 12 representing the years 2000–2100). The data were downloaded from the PCMDI – LLNL (http://www-pcmdi.llnl.gov/). Due to data limitations, however, the results are only presented for the 12 best-performing models for the historical run and for the RCP4.5 and RCP8.5 scenarios. The moisture convergence (C) for each model is obtained from P and E, as the model is balanced throughout the runs.

Monthly data from the National Center for Environmental Prediction, National Center for Atmospheric Research (NCEP/NCAR) 20th Century reanalysis dataset (Compo *et al*. 2011) are used to calculate the water budget for a period of 150 years from January 1870 until December 2000. These data comprise of surface level precipitation (P) and Evaporation (E). In addition, as the precipitation estimates over land areas in the GPCP are reasonably realistic, due to the merging of IR and microwave sensor estimates with gauge precipitation estimates, (Adler *et al*. 2003), GPCP estimates for both land and ocean are utilized in this study.

2.1.2 Water balance components

The atmospheric water budget equation (Peixoto and Oort, 1992), can be written as:

$$< \partial W/\partial t > + < \nabla . Q > = < E - P > \quad (1)$$

where P is precipitation, E is evaporation, W is precipitable water content, Q is vertically integrated moisture flux vector, and $\nabla \cdot Q$ its divergence. The angled brackets denote the area average. On longer timescales, (monthly or seasonal), under near equilibrium conditions, the time change of the local available precipitable water content is negligible in comparison with variations of large-scale convergence and evaporation (Oki *et al*., 1995; Trenberth, 1991; Trenberth and Guillemot, 1998; Trenberth, 1999; Trenberth, *et al*. 2005; Prasanna and Yasunari (2008, 2009, 2011)).

The local change of precipitable water content can be written as

$$<\partial W/\partial t> \approx 0 \quad (2)$$

Then, we can approximate:

$$C = P - E \quad (3)$$

Where, $C = -<\nabla \cdot Q>$ and C is the vertically integrated moisture convergence from the ground (surface pressure level) to the top of the atmosphere (TOA). C in the reanalysis and CMIP5 models is obtained from the atmospheric water balance equation [C = P − E], as the components are balanced in the coupled model runs. The sign of convergence and divergence are reversed in this study for convenience. E in the observation case is obtained from the 20th Century reanalysis (see first panel of Fig. 4).

3. RESULTS

3.1 Atmospheric hydrological cycle over South Asia

In this paper, 29 model simulations from the CMIP5 results were analyzed. The 12 models that performed best over the South Asian region were selected for creating reliable future projections of temperature and the hydrological cycle. This section discusses in detail the comparison of the models' simulations with the 20th Century reanalysis and reveals the model based climate change projections based on the RCP4.5 and RCP8.5 scenarios. The better performing models were selected based

on the mean and CV (Fig. 1); and the models which best simulated the area averaged seasonal mean precipitation and CV over south Asia (0–5N; 65–100E) were selected for future projections. The criteria were relaxed for certain models in order to include an adequate number of models in the study. By choosing models using this method, the selection of models that performed badly over the South Asian monsoon region was avoided.

3.1.1 Observed and simulated: Temperature, Precipitation, Evaporation and Convergence (P-E) climatology

The large-scale South Asian monsoon temperature, precipitation, evaporation and convergence (P-E) patterns in the summer (JJAS), as simulated by the 12 coupled models, are shown in Figs. 2, 3, 4 and 5 respectively. For the purpose of comparison, the long-term means of seasonal precipitation, evaporation, temperature and convergence (P-E) were computed based on the 20th Century reanalysis dataset and the 1850–2000 (historical dataset) control simulations. The simulated rainfall patterns were also compared with the observed precipitation of GPCP (Global Precipitation Climatology Project) (Adler *et al*. 2003), for the period 1980–1999 and for the 20th Century reanalysis dataset 1850–2000.

Most models simulated the observed temperature climatology for the JJAS season (Fig. 2) and the higher seasonal mean temperature over the Indian land mass. A few models showed a higher temperature over India, namely: ACCESS, CNRM, CSIRO, GISS, HadGEM2-ES. The remaining models simulated close to the observed seasonal mean temperature pattern.

Although most models simulated the general maximum precipitation over the west coast of India and the Bay of Bengal, some missed the rainfall maximum in the equatorial Indian Ocean. Only a few models realistically simulated the observed maximum rainfall during the monsoon season (in the context of the Indian monsoon) along the west coast of India and the North Bay of Bengal and adjoining northeast India. These models were: ACCESS, CNRM, HadGEM2-ES and MIROC5 and to some extent Can-ESM, GFDL-ESM2M, GISS, MPI-ESM and NOR-ESM (Fig. 3). The reason for

this could be linked to the coarse resolution of the models and their lack of ability to simulate the heavy rainfall over these regions due to the steep orography.

The evaporation and moisture convergence (P-E) pattern was not realistically simulated by many models with the exception of: ACCESS, CNRM, HadGEM2-ES, MIROC5, and to some extent Can-ESM, GFDL-ESM2M, GISS, MPI-ESM and NOR-ESM (Figs. 4 and 5).

A few models capture the equatorial Indian Ocean precipitation maximum due to the increased evaporative flux as well as the convergence (P-E). These models are: ACCESS, Can-ESM, CSIRO, GFDL-ESM2M and MIROC-5, and to some extent GISS, INMCM, MPI-ESM and NOR-ESM (Figs 4 and 5), which was also evident from the moisture convergence (P-E) pattern (Fig. 5). However, large inter model differences are evident among the models.

3.1.2. Climate Change Simulations of atmospheric water balance over South Asia in the selected 12 AOGCM

The current generation of climate models reproduced the major features of the observed distribution of T, P, E and C (P-E) to some extent, but there was a considerable scattering among the models' results and between the simulated and observed values. The time series of the simulated South Asian summer monsoon region's seasonal temperature, rainfall, evaporation and convergence (P-E) from the historical, RCP4.5 and RCP8.5 scenarios, are shown in Figs. 6, 7, 8, and 9. The colored lines represent area-averaged values of T, P, E and C (P-E) for each model, respectively. As might be expected in the historical run, and in experiments with observed greenhouse forcing, the simulations of all models show very little increase in T, P, E and C (P-E). However, the transient simulations with the RCP4.5 and RCP8.5 scenarios show a marked increase in temperature and monsoon precipitation towards the end of 21st century, becoming particularly obvious after the 2050's. As evident in Figs. 7 and 8, although all models show an increase in precipitation over South Asia, there is a considerable spread among the models in the magnitude of change, unlike that of simulations of temperature increase (Fig. 6).

The increase in monsoon precipitation and associated atmospheric water balance components in the model simulations using the historical period, and the subsequent changes in the future (RCP4.5-historical and RCP8.5-historical) for JJAS over the South Asian monsoon domain, are shown in Figs. 7, 8, and 9. All models show a general consensus of increase in precipitation associated with an increase in AWB components (evaporation and convergence). The increase in mean precipitation is mainly due to the increase in the projected moisture convergence (Fig. 9), which may be attributed to the increased horizontal transport of moisture from the oceans towards the land through advection (Ueda *et al*. 2006; Kripalani *et al*. 2007; Prasanna and Yasunari, 2011). However, the role of evaporation alone through in-situ surface hydrological processes is limited in intensifying the hydrological cycle and the projected increase in the mean precipitation is evident in all the AOGCM results, while increases are large for moisture convergence but not for evaporation (figs.8 and 9).

3.1.3 Future spatial changes of patterns of the atmospheric water balance over South Asia in RCP 4.5 and RCP 8.5

Future rainfall changes on the broad regional scale described above are examined further to see their spatial manifestations over the South Asian region. The RCP4.5 and RCP8.5 forced changes in monsoon rainfall were computed for a 100-year period for all models, from 2000 to 2100, and for a 150 year period from 1850 to 2000 in the historical. The changes are expressed as departures for the temperature and water budget components P, E and C (P-E) (Figs. 10, 11, 12, 13, 14, 15, 16, 17) for both RCP4.5 and RCP8.5 scenarios with reference to the present climate period (1850–2000) of historical AOGCM simulations; considered as the baseline climate.

The surface temperature change in RCP8.5 is higher than in the RCP4.5 scenario due to an accelerated warming in RCP8.5 (Figs. 10 and 11). The increase in temperature is larger over the continental regions, and the northern hemispheric land mass is heated faster than the oceans.

As evident from Figs. 12 and 13, most of the models project an enhanced precipitation during the monsoon season, particularly over the monsoon active parts

of India. However, the magnitudes of projected changes differ considerably from one model to the other. There is very little change (or none) noted in the monsoon rainfall over drier parts of India. It is important to note here that the maximum change in rainfall occurs over the climatologically high rainfall regions of India. The implication of such a change over this region needs to be carefully assessed in future studies.

The magnitude of the increase is larger in the RCP8.5 scenario than in the RCP4.5 scenario, but the pattern of increase does not show any significant difference. Most of the models' simulations show a general decrease in precipitation over the equatorial Indian Ocean, which is evident from future precipitation pattern changes (Figs. 12 and 13), associated with the decrease in both E and C (P-E) (Figs. 14, 15 and 16, 17). However, the models' simulations show an increase in precipitation over India (Figs. 12 and 13) associated with an increase in E and C (P-E) (Figs. 11 and 12). Generally, an increase in precipitation over the South Asian region is accompanied by an increase in convergence, as well as an increase in evaporation over the land area. The enhancement of precipitation over India is also accompanied by an increase in the Western North Pacific monsoon. Being one of the major heat sources of the Asian monsoon, the western North Pacific monsoon suppresses the equatorial Indian Ocean precipitation (Prasanna and Annamalai, 2012), which is partly responsible for an increase in precipitation over the Indian Monsoon region via the northwest propagation of twin Rossby waves from the equatorial Indian Ocean.

The increase in the moisture convergence flux could be attributed to the increase in the lower tropospheric specific humidity, which is evident in all models (figure not shown). The increase of P in the models, due to an increase of C (P-E), could be due to an increase in the lower tropospheric precipitable water component (PW), and not due to the wind convergence.

There are large projected surface temperature increases (Figs. 10 and 11) over the monsoon region. This increases the water holding capacity of the atmosphere, and the hydrological cycle over the South Asian monsoon region is thereby enhanced for the RCP4.5 and RCP8.5 scenarios in the model projections for the 21st century climate simulations. The homogeneous increase of surface temperatures over the

tropics in the models may have decreased the continental north-south temperature gradient over the South Asian region, which could be a possible explanation for the decrease in the wind convergence in the RCP4.5 and RCP8.5 scenarios.

3.1.4 Future projection of scenarios of variability of atmospheric water balance components

Apart from changes in mean state, the likely changes in the variability of monsoon rainfall and water balance components in the future would have a profound impact on various facets of human activities. Any increase in the year-to-year variability (interannual variability) of the monsoon will lead to the more frequent occurrence of large-scale seasonal anomalies and associated drought and floods. With respect to this, we examined the likely changes in the variance of T, P, C, and E in the RCP4.5 and RCP8.5 scenarios from 2000 to 2100. The standard deviation is taken here to represent the variance of the T, P, C, and E and is computed on a 31-year sliding window during the entire period of simulations. The results are presented in the form of a time series of variance for temperature in Fig. 18; the three components of water balance (P, C, and E) for the RCP4.5 simulation in Fig.19 and for the RCP8.5 in Fig. 20. The standard deviation values for the historical runs between 1850 and 2000 are also shown in Fig.19 and Fig. 20 for a comparison of the changes in the variance of temperature and in each water balance component (P, C and E) within the RCP4.5 and RCP8.5 scenarios. Most of the models showed a general tendency of an increased variance in the later part of 21st century. However, only a few models showed such a systematic increase in variance into the future. It can, therefore, be stated that there is as yet no conclusive evidence or general consensus among the models of the future changes related to an enhanced variability in monsoon rainfall.

4. DISCUSSION AND CONCLUSION

This paper evaluates the performance of 12 state-of-the-art coupled atmosphere-ocean general circulation models (AOGCMs) in their representation of the South Asian regional monsoon characteristics of temperature, rainfall and atmospheric water balance components (P, E, C (P-E)). Based on modeling experiments conducted for RCP4.5 and RCP8.5 scenarios, regional climate change projections of rainfall and water balance components up until the end of the 21st century were presented. The major conclusions of the study are as follows:

(1) The AOGCMs, despite their relatively coarse resolution, have shown a reasonable skill in depicting the observed hydrological cycle over the South Asian region.

(2) Model simulations under scenarios of increased greenhouse gas concentrations indicate a marked increase in both rainfall and atmospheric water balance components, becoming particularly obvious after the 2050's. There is, however, a considerable inter-model disparity related to monsoon rainfall projections and the atmospheric water balance.

(3) Spatial patterns of rainfall change projections indicate a maximum increase over the Indian monsoon region and the western North Pacific, associated with an intensification of the atmospheric water balance components over the domain.

(4) There is no clear evidence of a substantial change in the variability of monsoon rainfall and atmospheric water balance over the next century.

(5) While the scenarios presented in this study are indicative of the expected range of rainfall and atmospheric water balance changes, it must be noted that the quantitative estimates still have large uncertainties associated with them.

REFERENCES

Adler, R.F., Huffman, G.J., Chang, A., Ferraro, R., Xie, P., Janowiak, J., Rudolf, B., Schneider, U., Curtis, S., Bolvin, D., Gruber, A., Susskind, J., Arkin, P., Nelkin, E. (2003) The Version 2 Global Precipitation Climatology Project (GPCP), Monthly Precipitation Analysis (1979-Present). J Hydrometeor 4: 1147-1167

Christensen, J.H., Hewitson, B., Busuioc, A., Chen, A., Gao, X., Held, I., Jones, R., Kolli, R.K., Kwon, W.T., Laprise, R., Magaña Rueda, V., Mearns, L., Menendez, C.G., Raisanen, J., Rinke, A., Sarr, A., Whetton, P. (2007) Regional climate projections climate change 2007: the physical science basis contribution of working group I to the fourth assessment report of the intergovernmental panel on climate change. In: S. Solomon, Qin, D., Manning, M., Chen, Z., Marquis, M., Averyt, K.B., Tignor, M., Miller, H.L. (eds). Cambridge University Press, Cambridge. p. 996

Compo, G.P., J.S. Whitaker, P.D. Sardeshmukh, N. Matsui, R.J. Allan, X. Yin, B.E. Gleason, R.S. Vose, G. Rutledge, P. Bessemoulin, S. Brönnimann, M. Brunet, R.I. Crouthamel, A.N. Grant, P.Y. Groisman, P.D. Jones, M. Kruk, A.C. Kruger, G.J. Marshall, M. Maugeri, H.Y. Mok, Ø. Nordli, T.F. Ross, R.M. Trigo, X.L. Wang, S.D. Woodruff, and S.J. Worley (2011) The Twentieth Century Reanalysis Project. Quarterly J. Roy. Meteorol. Soc., 137, 1-28. DOI: 10.1002/qj.776

IPCC (1996) Climate Change 1995: The Science of Climate Change Contribution of Working Group I to the Second Assessment Report of the Intergovernmental Panel on Climate Change. In: Houghton JJ, MeiroFilho LG, Callander BA, Harris N, Kattenberg A, Maskell K (eds). Cambridge University Press, Cambridge United Kingdom and New York, NY, USA, 572 pp

IPCC (2001) Climate Change 2001: The Scientific Basis Contribution of Working Group I to the Third Assessment Report of the Intergovernmental Panel on Climate Change. In: Houghton JT, Ding Y, Griggs DJ, Noguer M, VanderLinden PJ, Dai X, Maskell K, Jhonson CA(eds). Cambridge University Press, Cambridge United Kingdom and New York, NY, USA, 881 pp

IPCC (2007) Climate Change 2007: The Physical Science Basis Contribution of Working Group I to the Fourth Assessment Report of the Intergovernmental Panel on Climate Change. In: S. Solomon, Qin, D., Manning, M., Chen, Z., Marquis, M., Averyt, K.B., Tignor, M., Miller, H.L. (eds). Cambridge University Press, Cambridge United Kingdom and New York, NY, USA, 996p

Kripalani, R.H., Oh, J.H., Kulkarni, A., Sabade, S.S., Chaudhari, H.S. (2007) South Asian summer monsoon precipitation variability: Coupled climate model simulations and projections under IPCC AR4. Theor Appl Climatol 90:133–159

Oki, T., Musiake, K., Matsuyama, H., Masuda, K. (1995) Global atmospheric water balance and runoff from large river basins. Hydrol Processes 9: 655–678

Peixoto, J.P. and Oort, A.H. (1992) Physics of Climate. Amer Inst Phys 520 pp

Prasanna, V., Yasunari, T. (2008) Interannual variability of Atmospheric water balance over South peninsular India and Sri Lanka during North East Monsoon season. Intl J Climatol 28:1997–2009

Prasanna, V., Yasunari, T. (2009) Time-space characteristics of seasonal and interannual variations of atmospheric water balance over South Asia. J Meteor Soc Jpn 87:263–287

Prasanna, V., Yasunari, T. (2011) Simulated Changes in the atmospheric water balance over south

Asia in the eight IPCC-AR4 coupled climate models. Theor and App Clim, 104:139-158

Prasanna, V., Annamalai, H. (2012) Moist Dynamics of Extended Monsoon Breaks over South Asia. J Clim, 25, 3810–3831

Trenberth, K. E. (1991) Climate diagnostics from global analyses: Conservation of mass in ECMWF analyses. J Clim 4: 707-722

Trenberth, K. E., Guillemot, C.J. (1998) Evaluation of the atmospheric moisture and hydrological cycle in the JRA-25 reanalyses. Clim Dyn 14: 213-231

Trenberth, K. E. (1999) Atmospheric moisture recycling: Role of advection and local evaporation. J Clim 12: 1368-1381

Trenberth, K. E., Fasullo, J. and Smith, L. (2005) Trends and variability in column integrated water vapor. Clim Dyn 24: 741-758

Ueda, H., Iwai, A., Kuwako, K., Hori, M.E. (2006) Impact of anthropogenic forcing on the Asian summer monsoon as simulated by 8 GCMs. Geophys Res Lett 33: doi: 101029/2005GL025336

Acknowledgments

The author would like to acknowledge the Director of the APCC for providing the facilities in which to carry out this work, and the many modeling centers for providing the model simulations for a period of approximately 300 years. The author would also like to acknowledge the PCMDI for archiving and providing the large datasets through their website (http://www-pcmdi.llnl.gov/). The diagrams used for this study have been prepared using the free software packages, GrADS, XMGRACE and Intel Fortran, and the computational work has been performed using the Cent OS operating system environment.

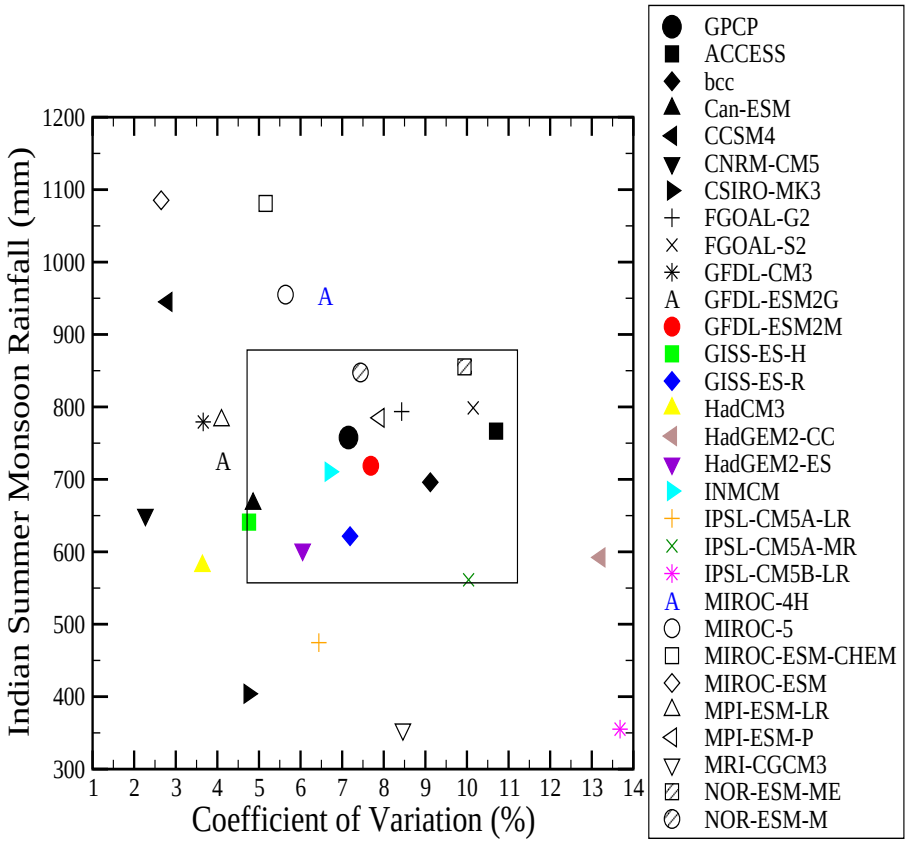

Figure 1 Scatter plot of ISMR (mm) and CV (%) from observation (GPCP Rainfall) and CMIP5 coupled climate model simulations over South Asia. Observation is denoted in black. The 29 different models are represented by different colors and shapes.

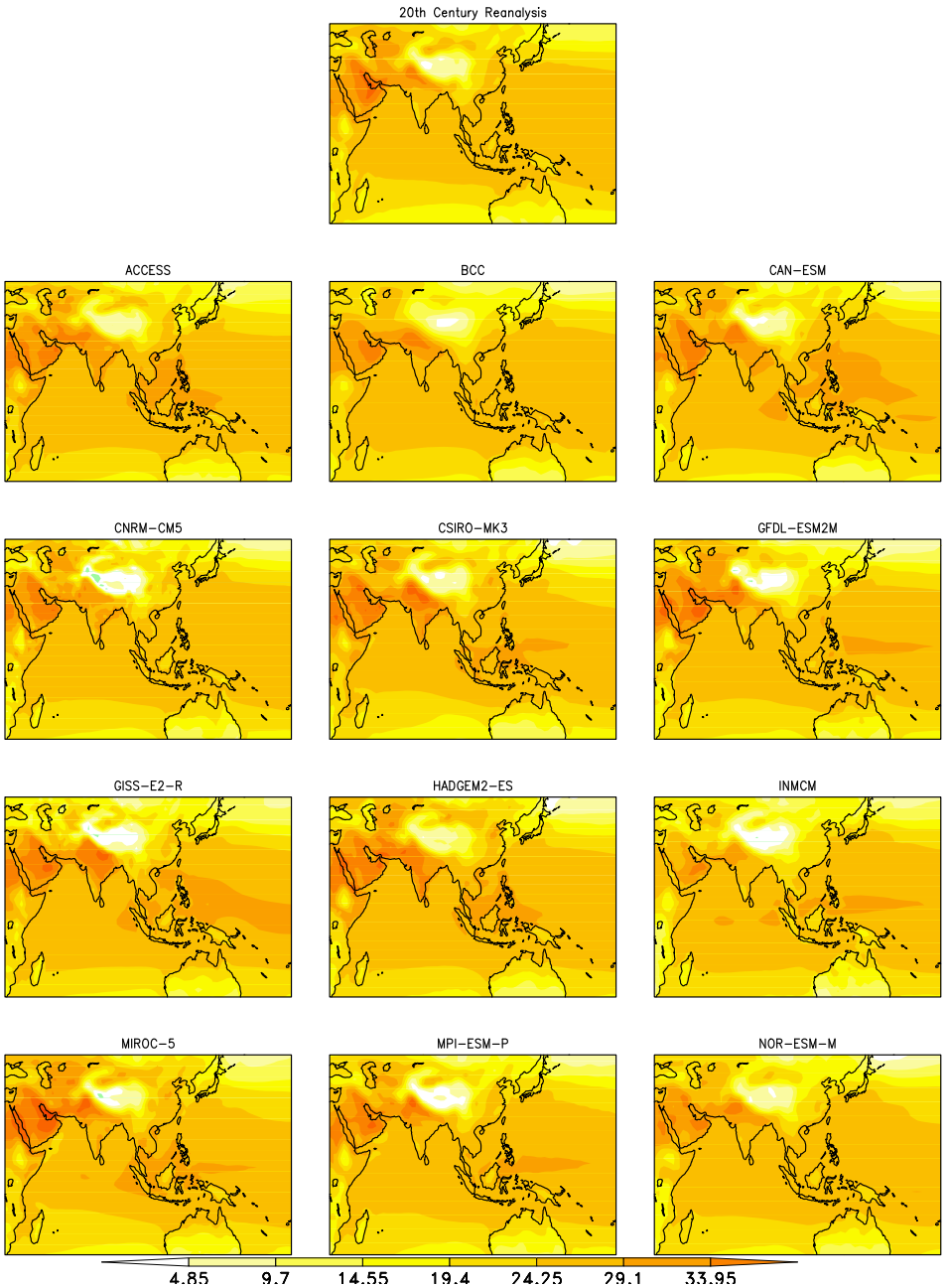

Figure 2 Climatological temperature simulations for JJAS season from CMIP5 climate models. Top panel shows 20th Century reanalysis climatology for the period 1850- 2000. (Unit for Temperature: Degree Centigrade)

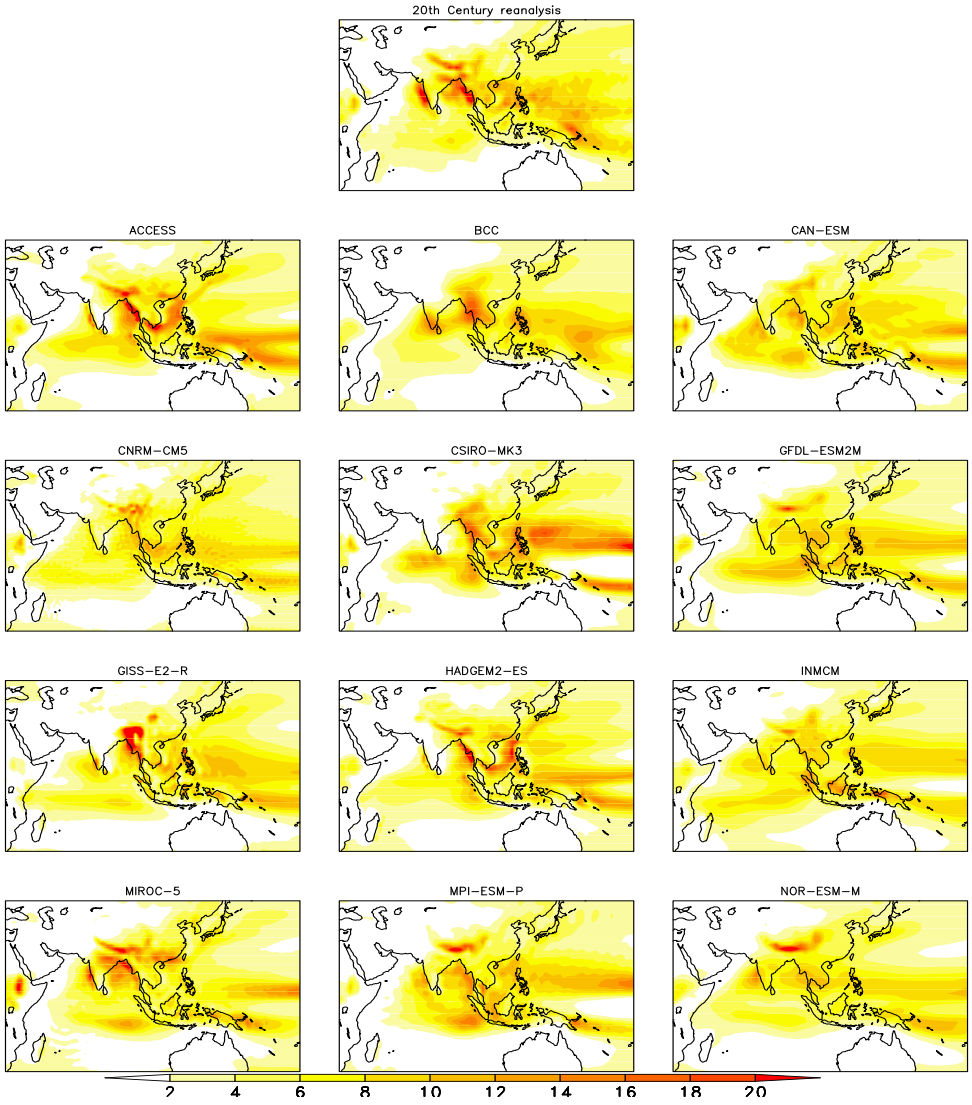

Figure 3 Climatological precipitation simulations for JJAS season from CMIP5 climate models. Top panel shows 20th Century reanalysis climatology for the period 1850- 2000. (Unit for precipitation: mm/day)

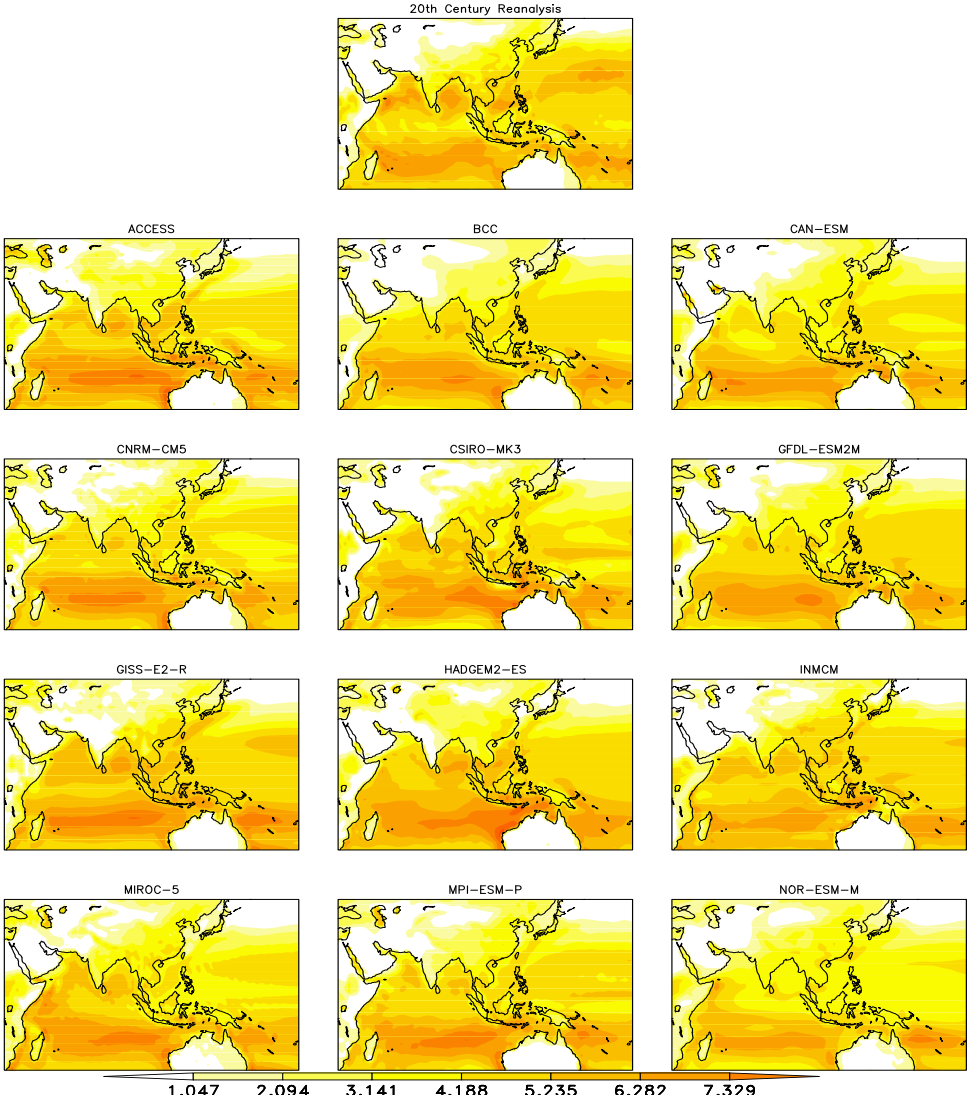

Figure 4 Climatological evaporation simulations for JJAS season from CMIP5 climate models. Top panel shows 20th Century reanalysis climatology for the period 1850- 2000. (Unit for evaporation: mm/day)

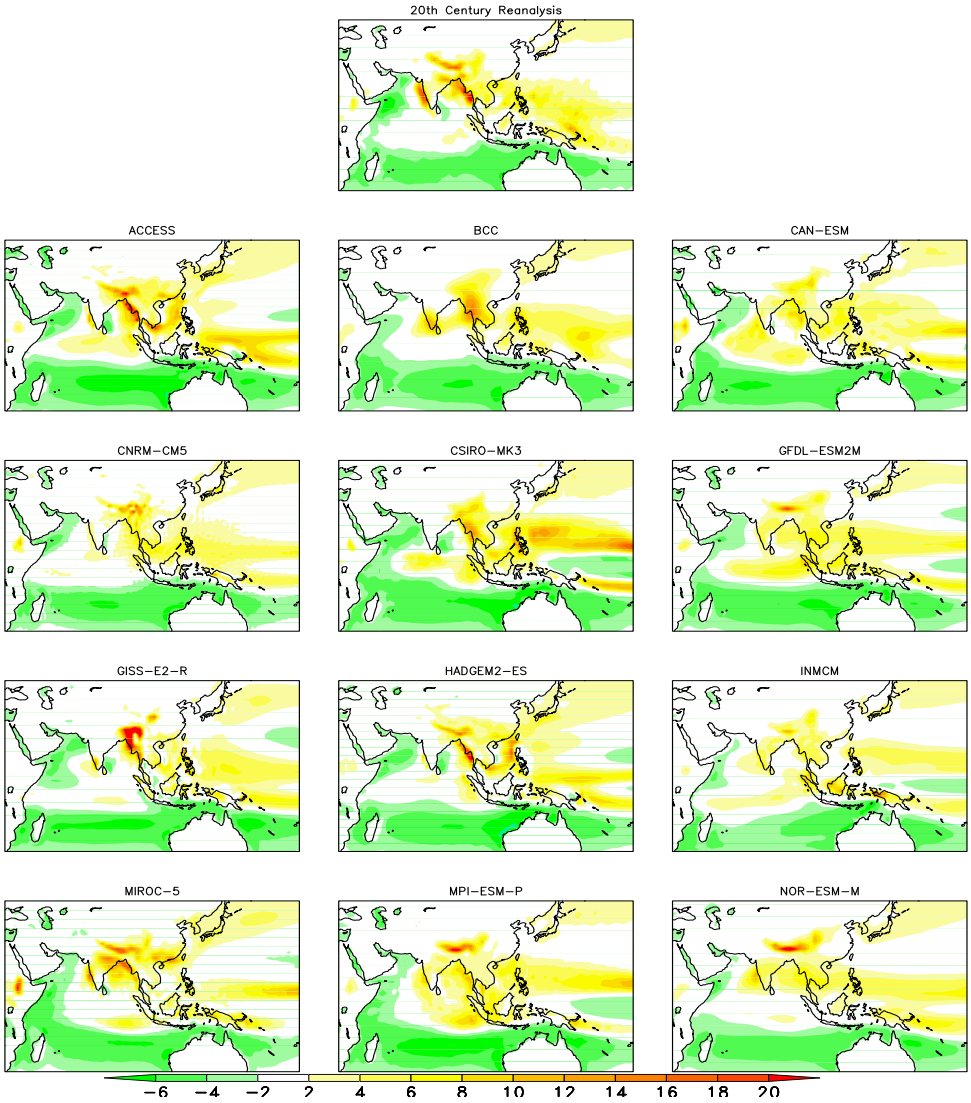

Figure 5 Climatological convergence (P-E) simulations for JJAS season from CMIP5 climate models. Top panel shows 20th Century reanalysis climatology for the period 1850- 2000. (Unit for convergence (P-E): mm/day)

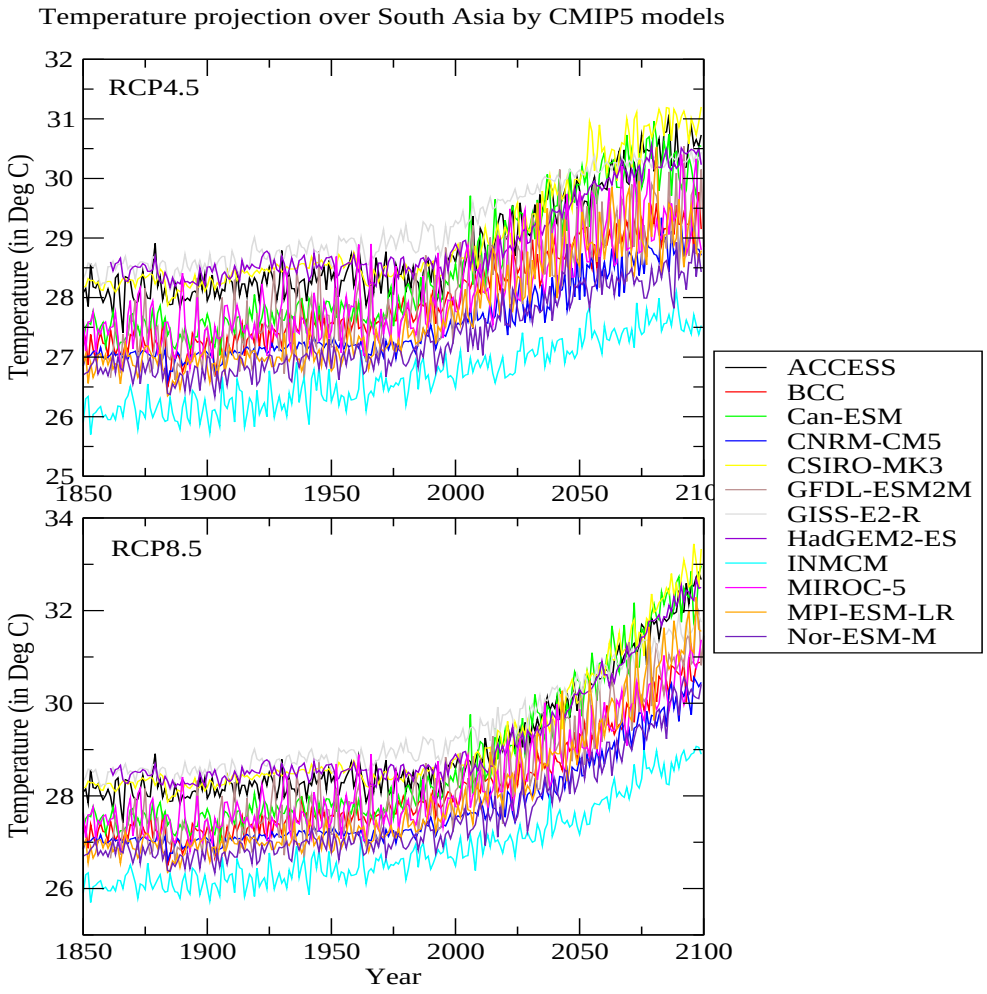

Figure 6 Time series of simulated temperature over South Asia in the historical, RCP4.5, and RCP8.5 runs. (Unit for Temperature: Degree Centigrade)

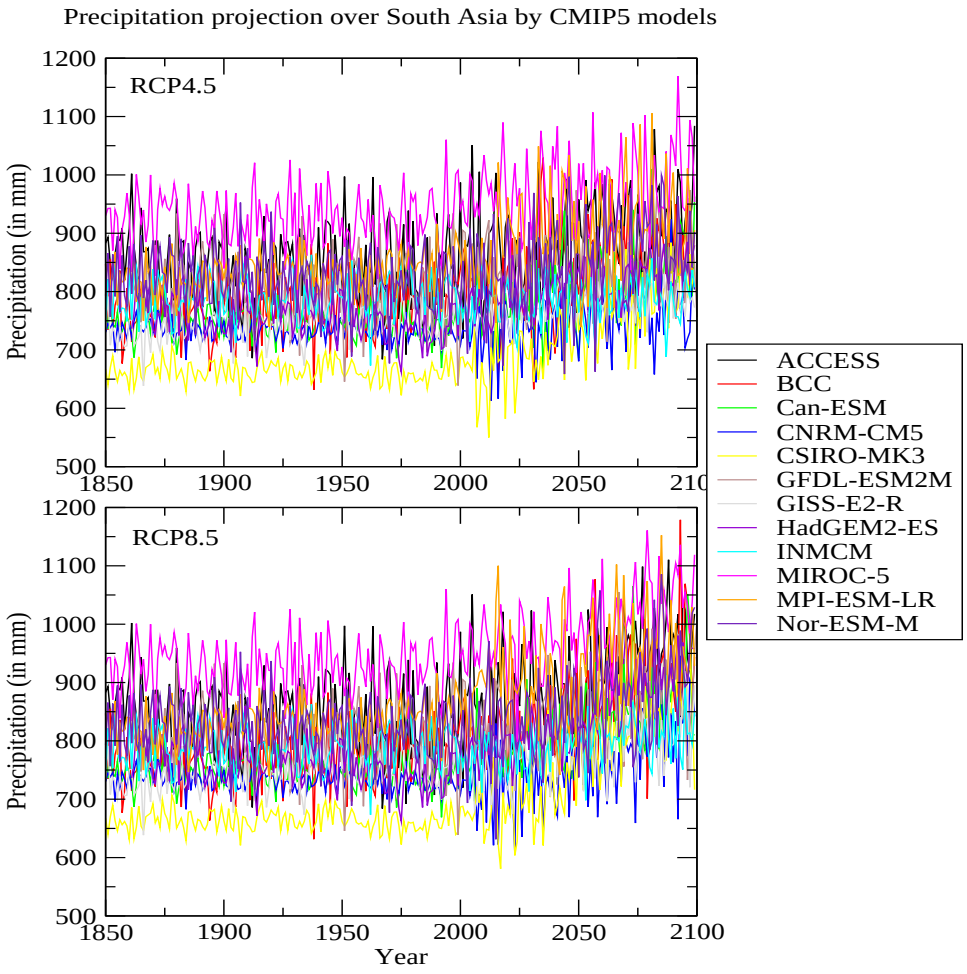

Figure 7 Time series of simulated precipitation over South Asia in the historical, RCP4.5, and RCP8.5 runs. (Unit for Precipitation: mm/day)

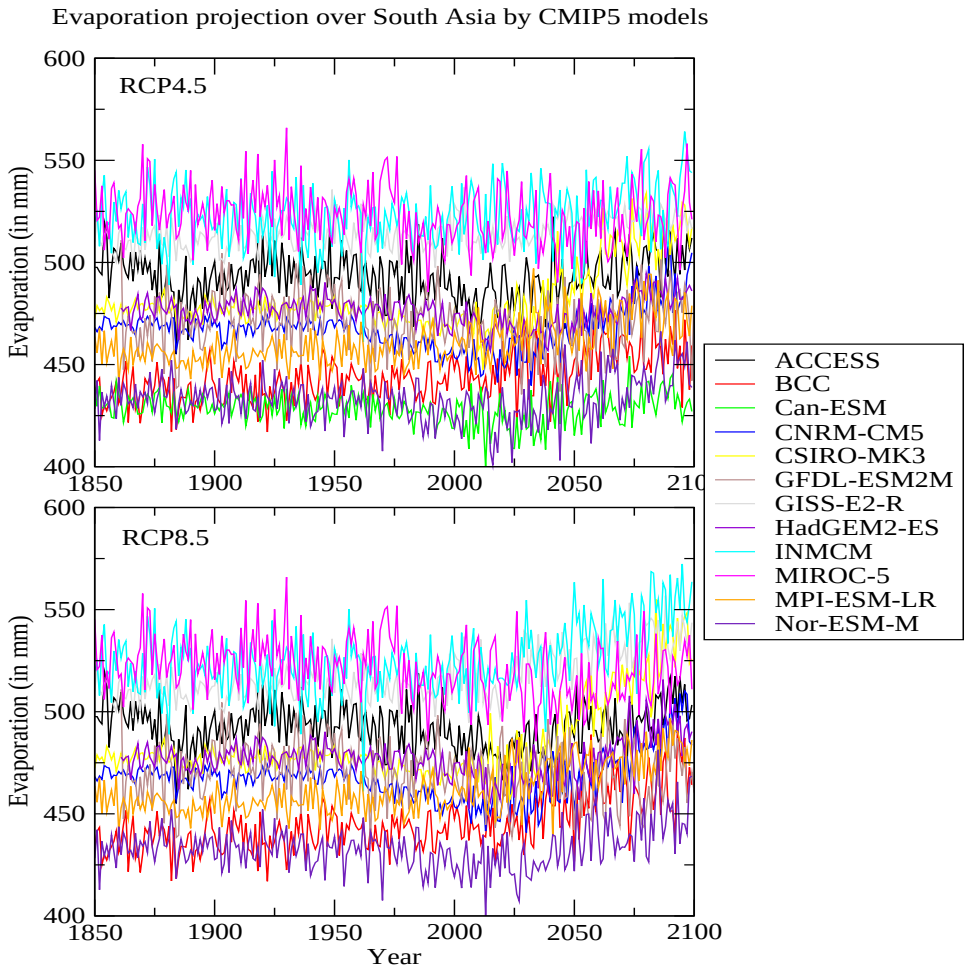

Figure 8 Time series of simulated evaporation over South Asia in the historical, RCP4.5, and RCP8.5 runs. (Unit for Evaporation: mm/day)

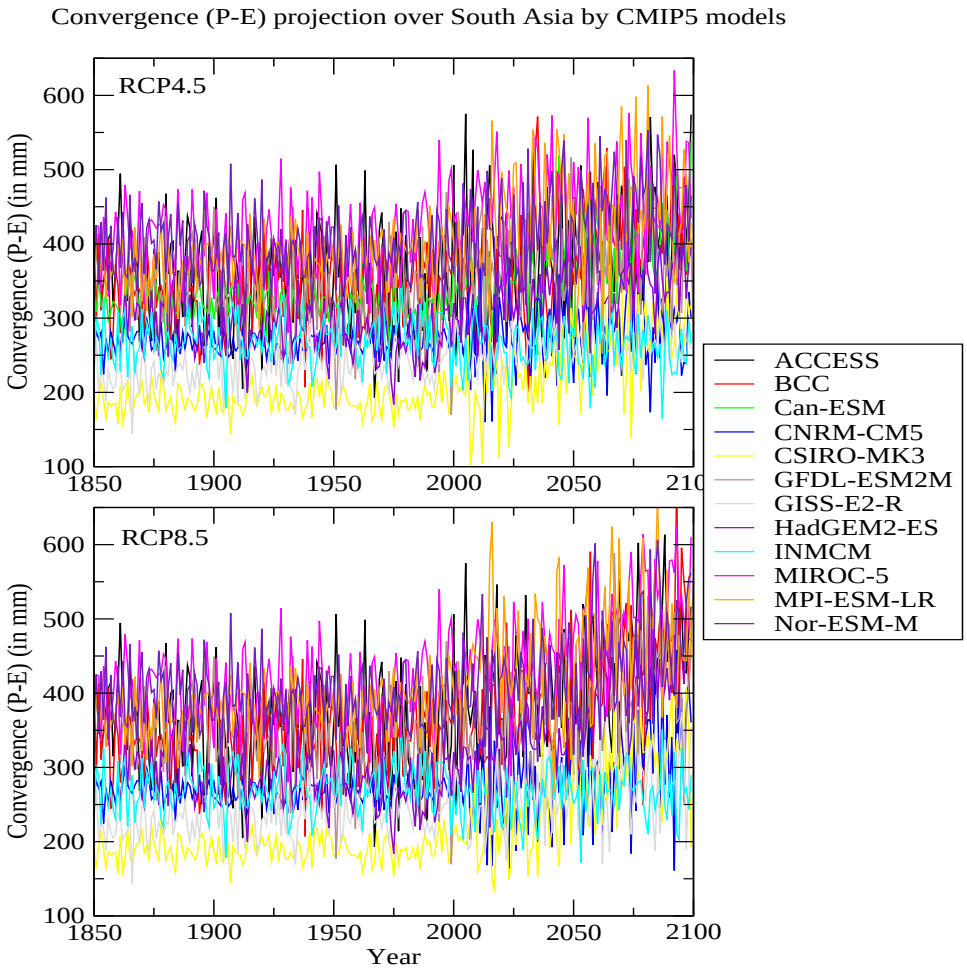

Figure 9 Time series of simulated convergence (P-E) over South Asia in the historical, RCP4.5, and RCP8.5 runs. (Unit for convergence (P - E): mm/day)

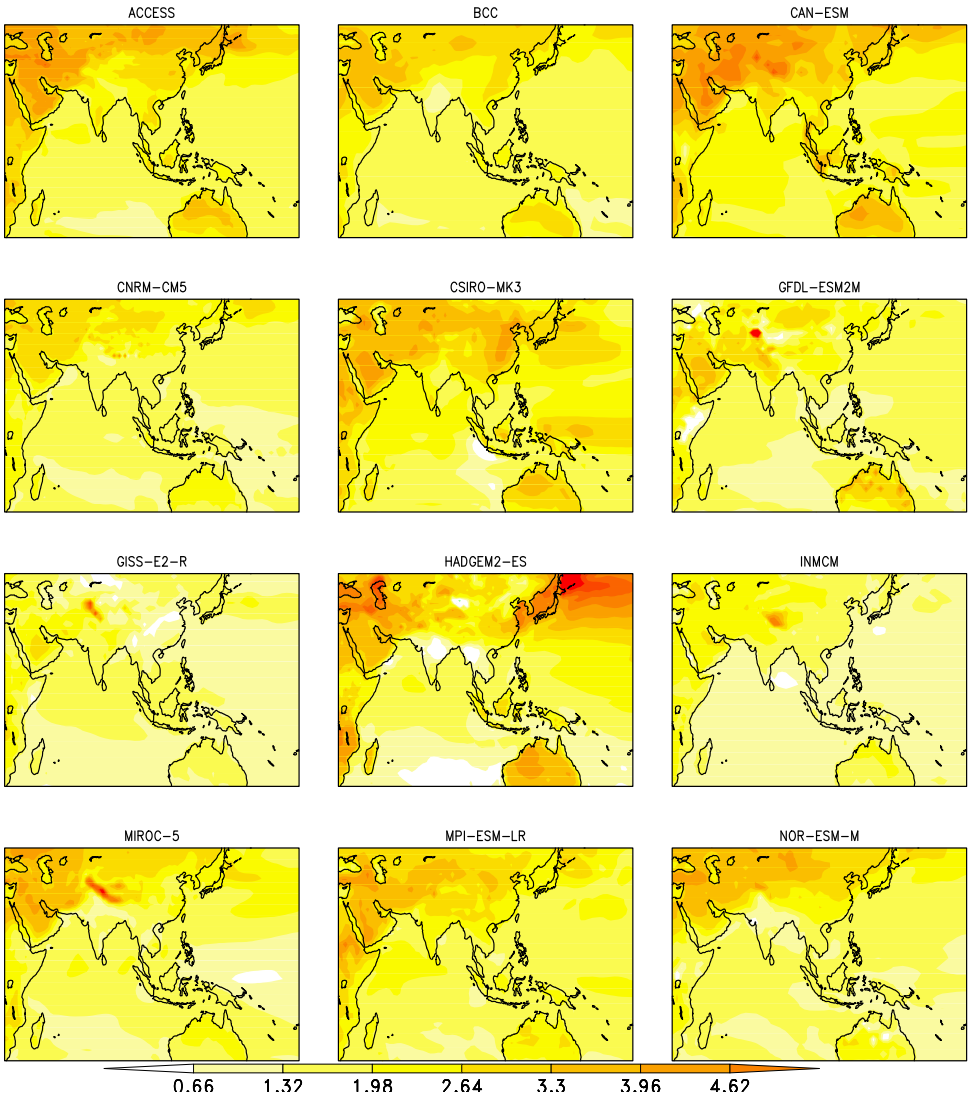

Figures 10 Spatial patterns of projected temperature changes (RCP4.5 – historical) in centigrade departure.

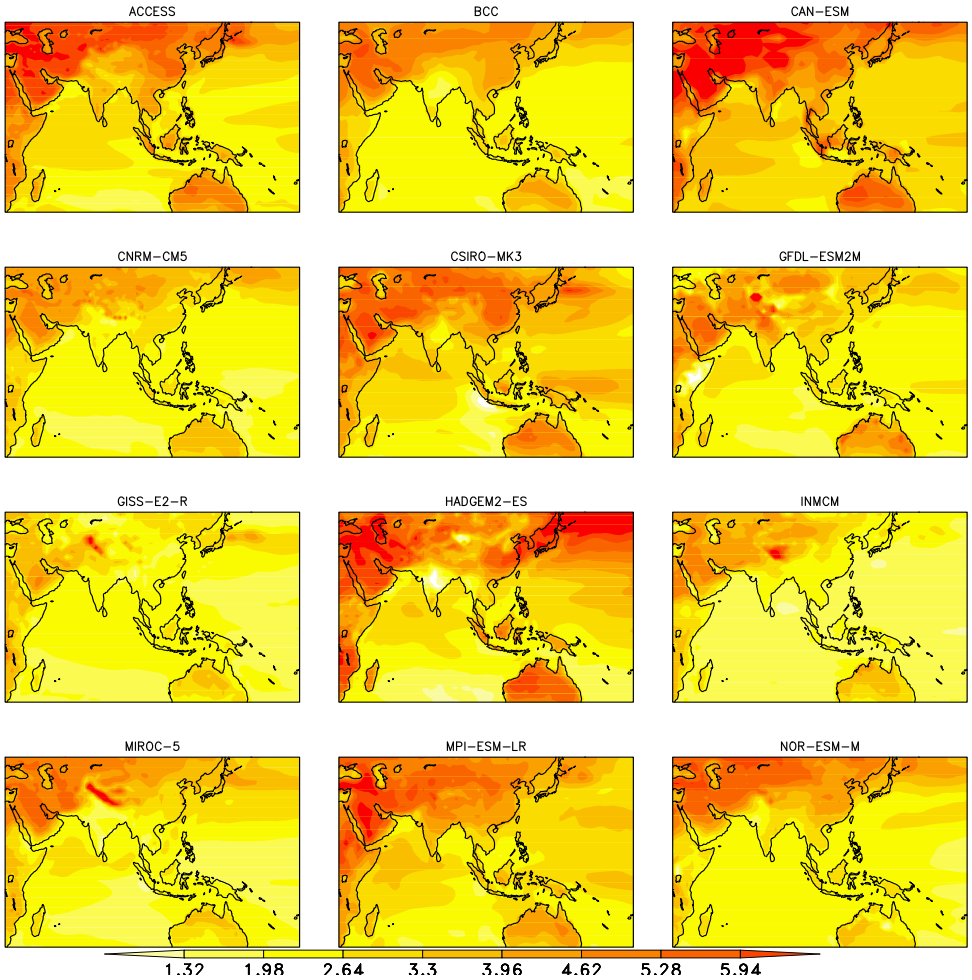

Figures 11 Spatial patterns of projected temperature changes (RCP8.5 – historical) in centigrade departure.

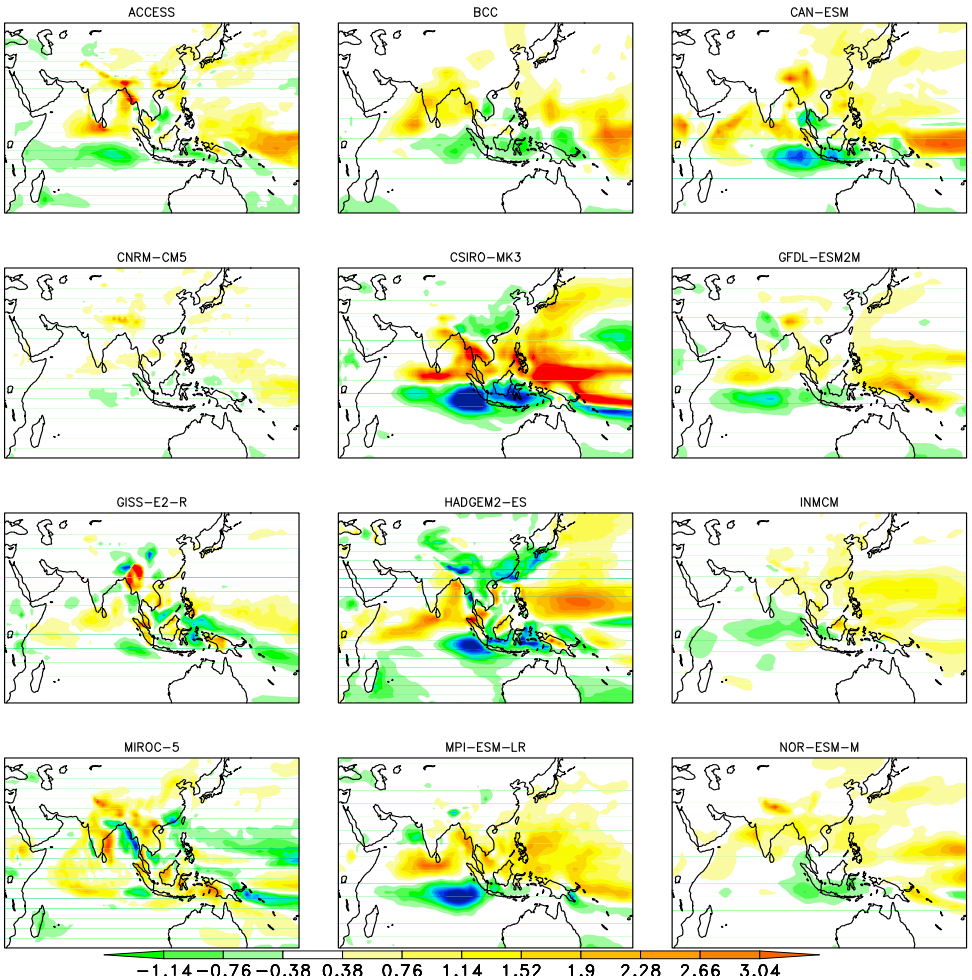

Figures 12 Spatial patterns of projected precipitation changes (RCP4.5– historical) in mm/day departure.

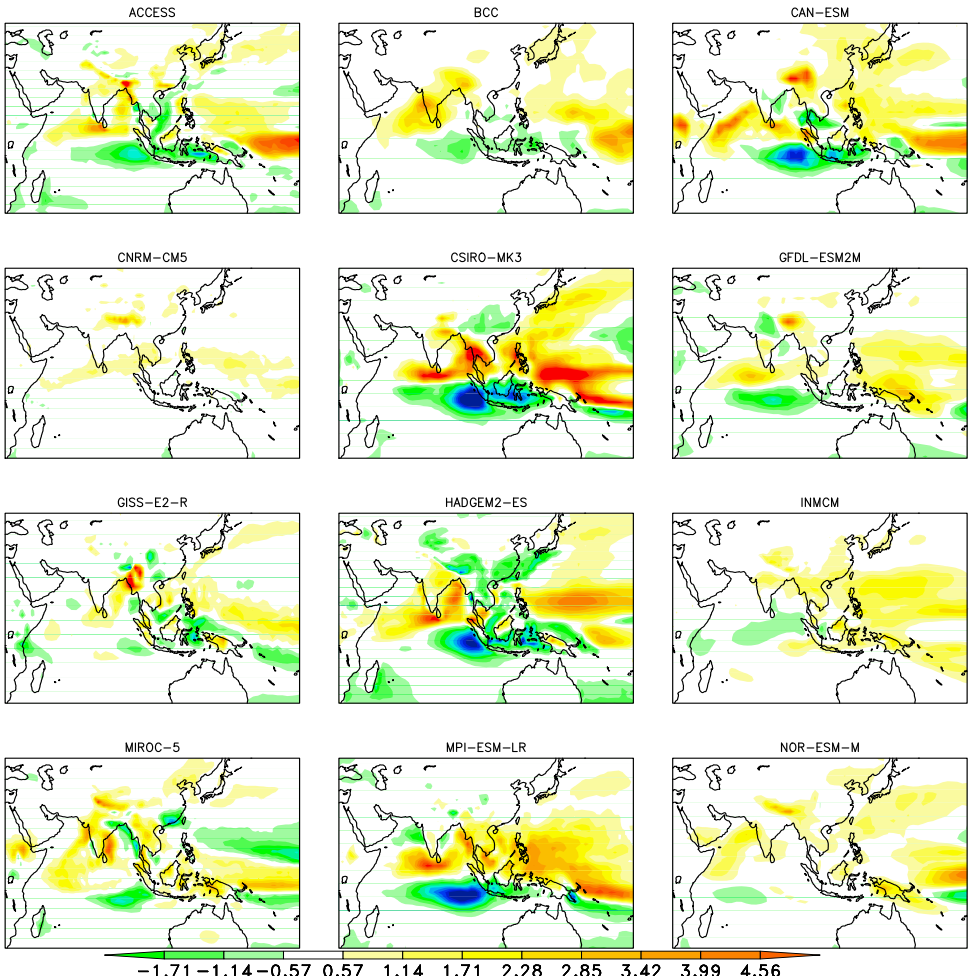

Figures 13 Spatial patterns of projected precipitation changes (RCP8.5– historical) in mm/day departure.

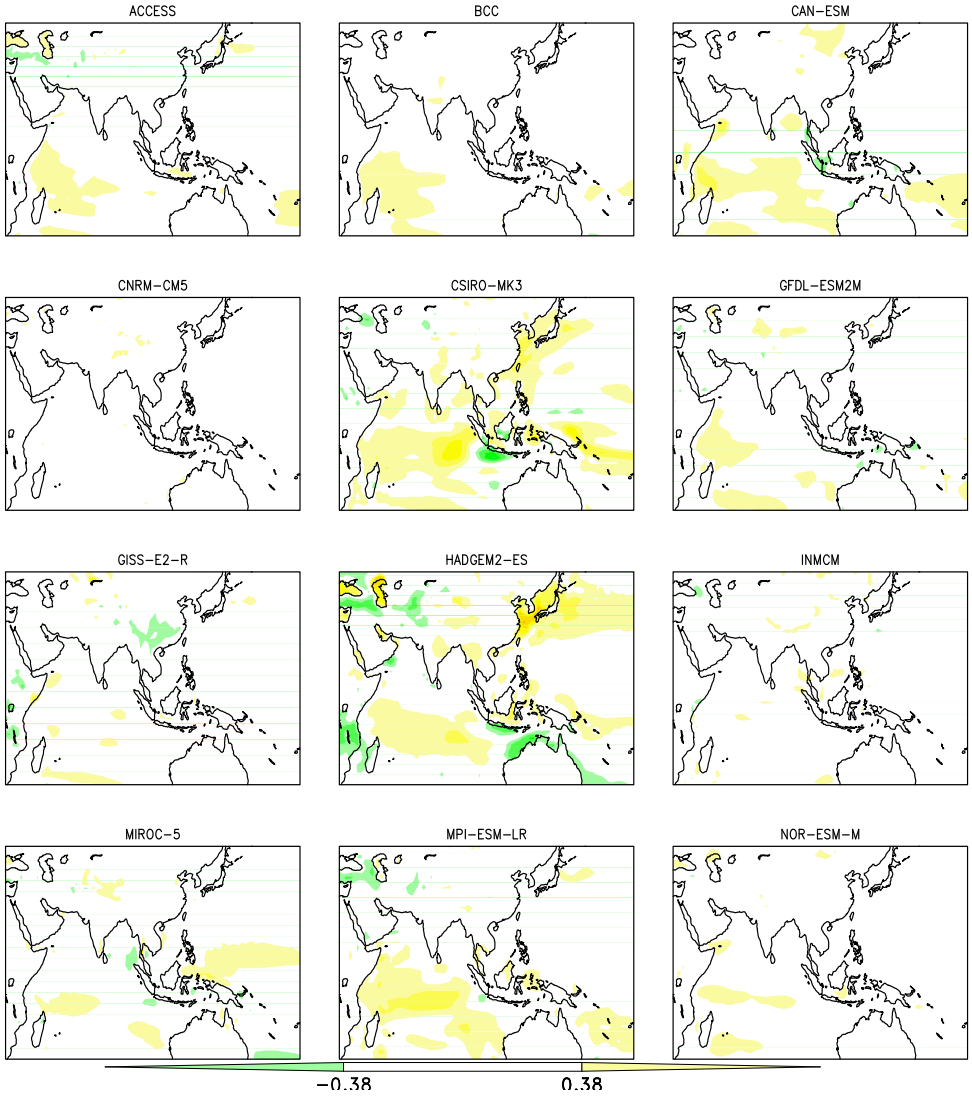

Figures 14 Spatial patterns of projected evaporation changes (RCP4.5– historical) in mm/day departure.

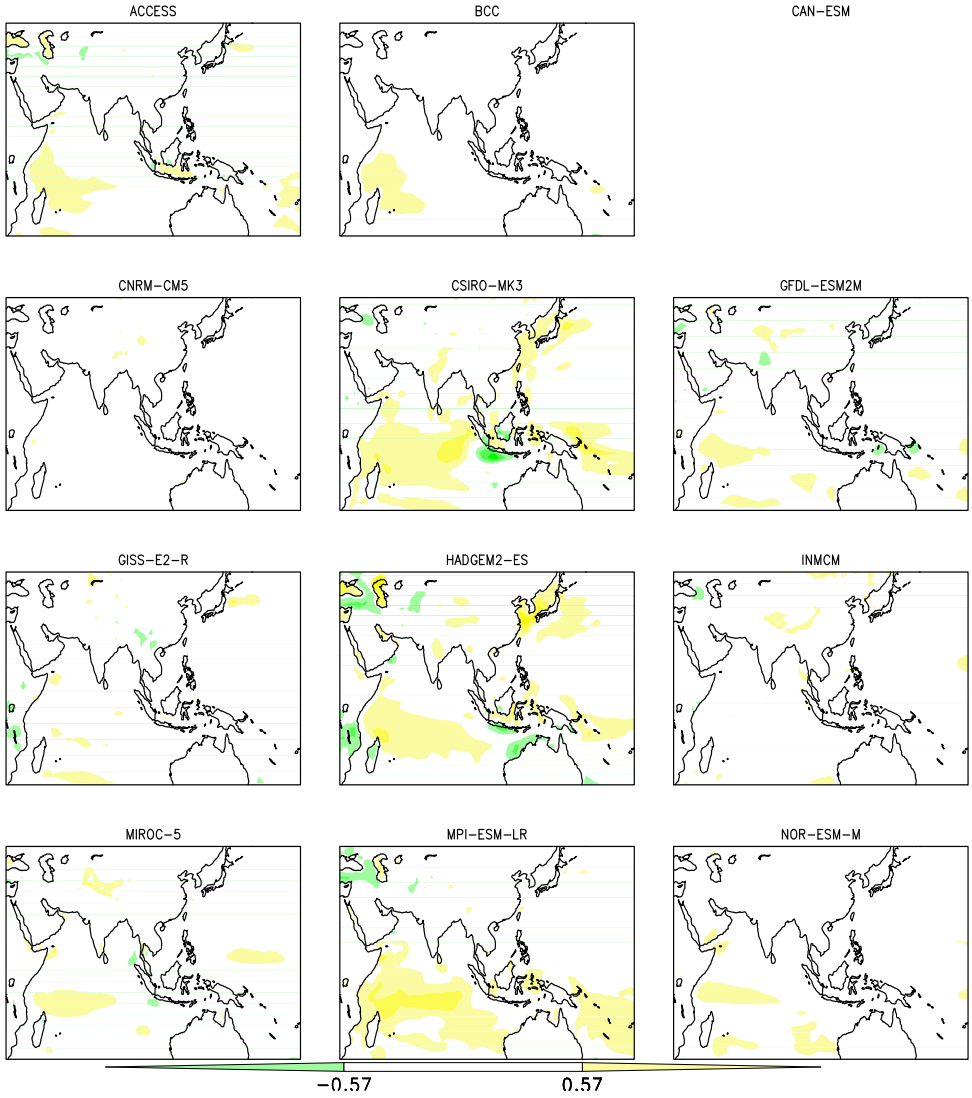

Figures 15 Spatial patterns of projected evaporation changes (RCP8.5– historical) in mm/day departure.

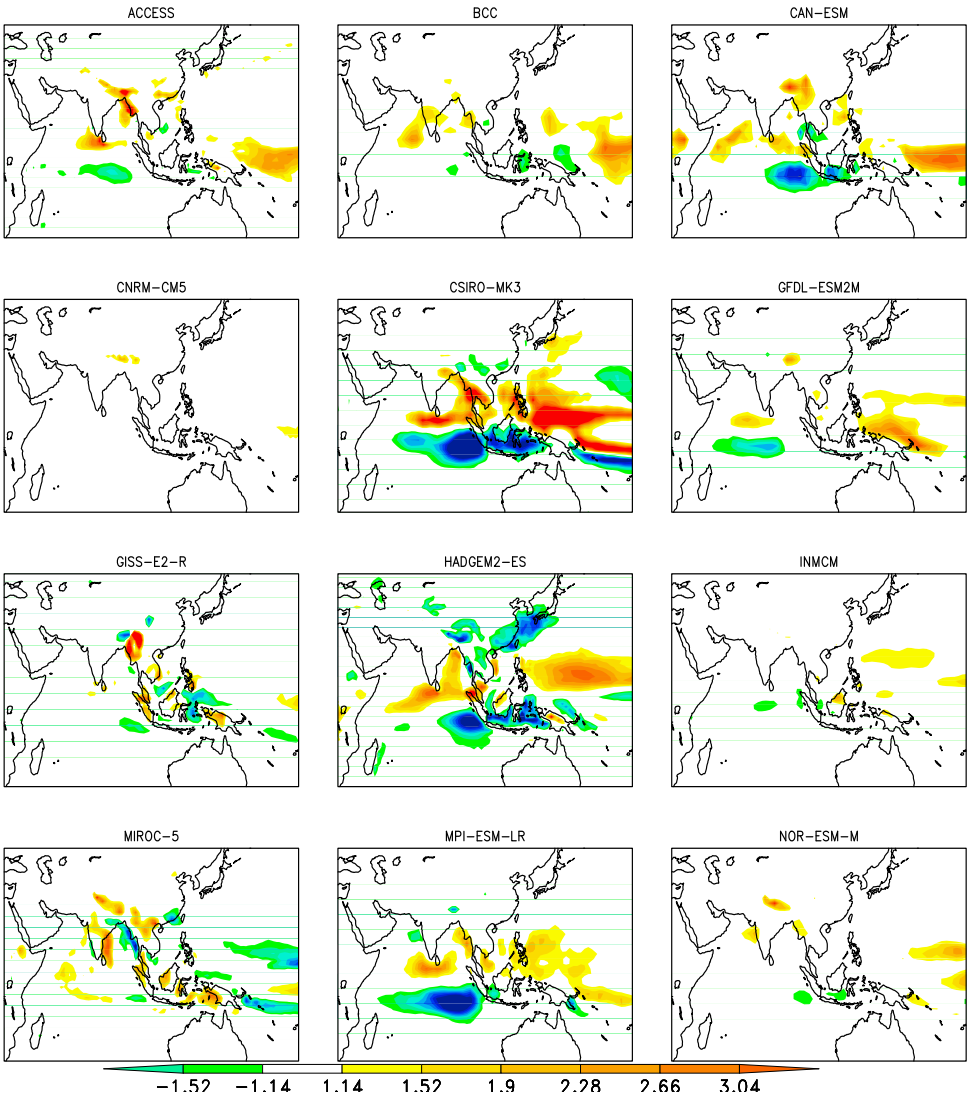

Figures 16 Spatial patterns of projected convergence (P-E) changes (RCP4.5– historical) in mm/day departure.

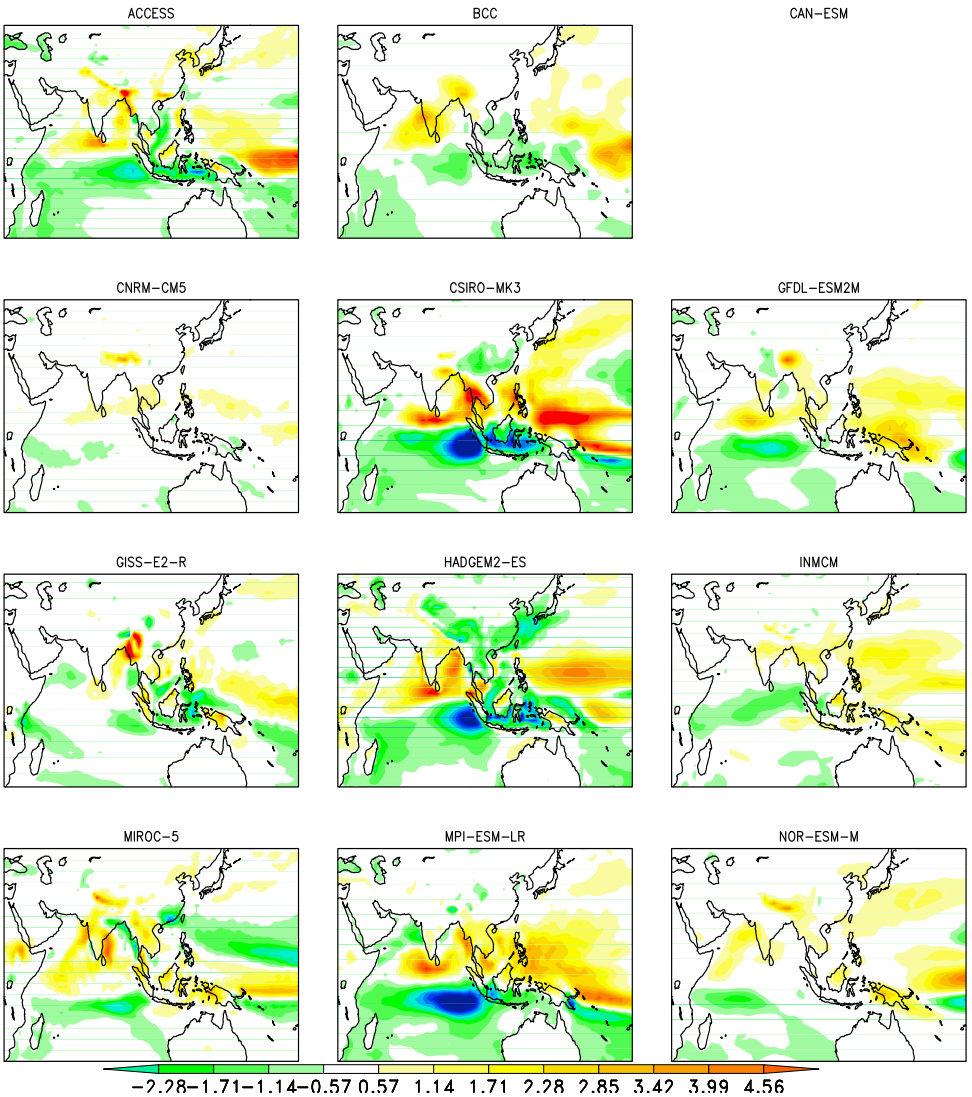

Figures 17 Spatial patterns of projected convergence (P-E) changes (RCP8.5– historical) in mm/day departure.

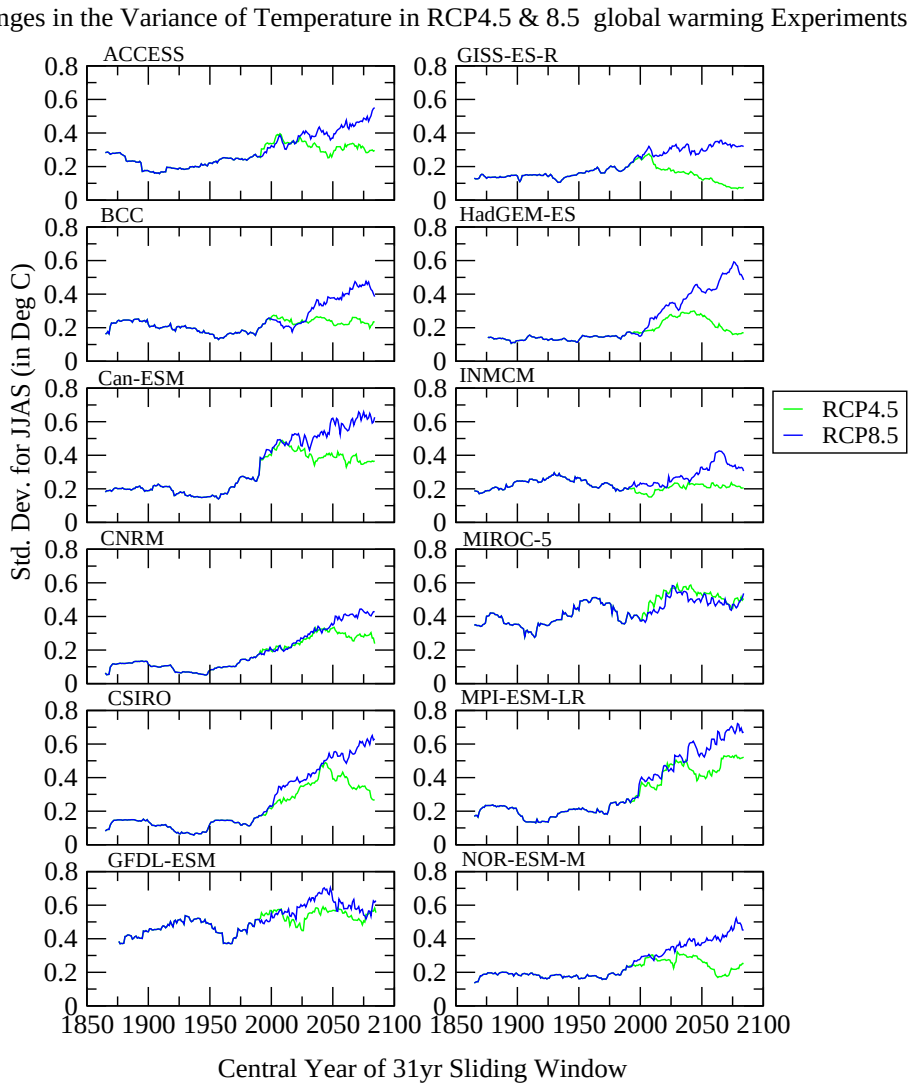

Figure 18 Future changes in the variance (time series from 1850 to 2100) of Temperature (deg Centigrade) (standard deviation is taken as a measure of variability) in different models for RCP4.5 and RCP 8.5 scenario runs. The blue lines denote standard deviation of temperature for RCP 4.5 in respective models; green lines indicate standard deviation of temperature for RCP 8.5 in respective models.

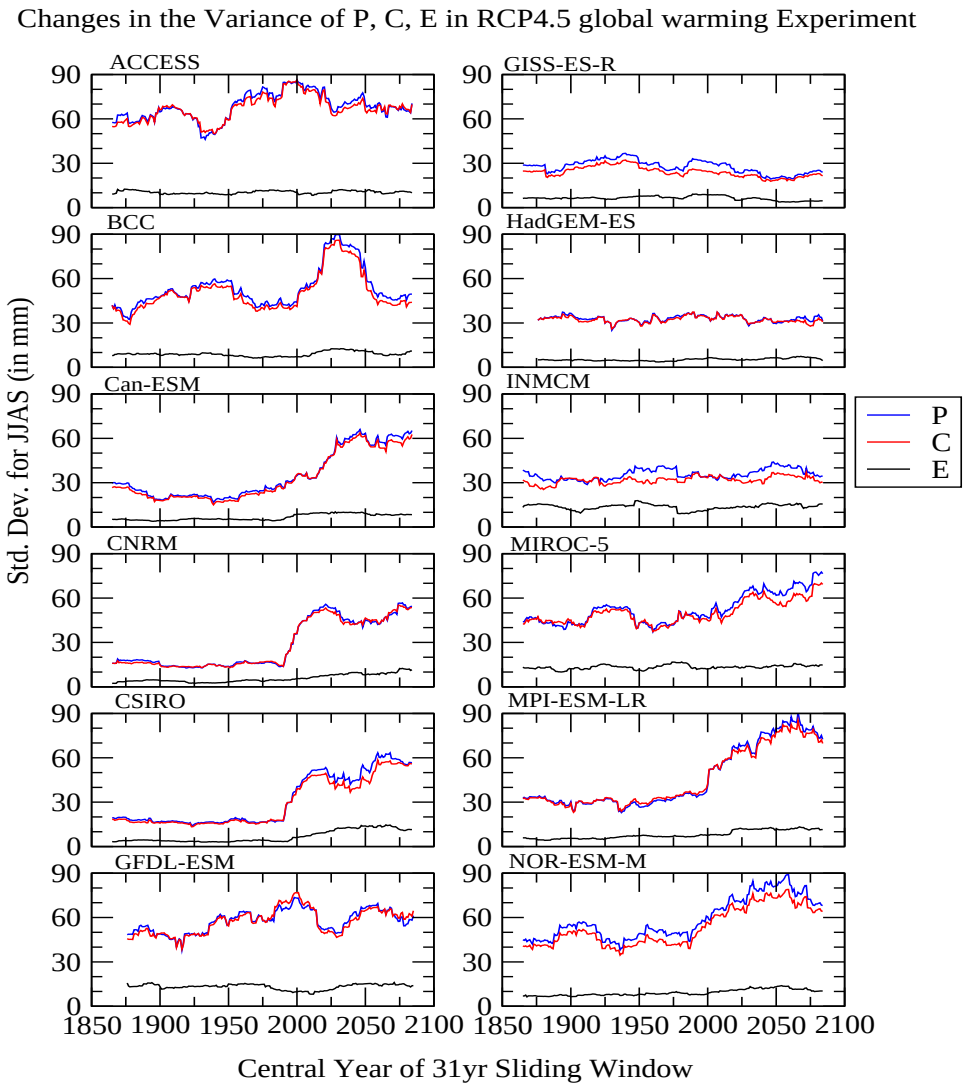

Figure 19 Future changes in the variance (time series from 1850 to 2100) of AWB components (P, C and E) (mm) (standard deviation is taken as a measure of variability) in different models for RCP4.5 scenario run. The blue lines denote standard deviation of precipitation in respective models; red lines indicate standard deviation of convergence; black lines indicate standard deviation of evaporation.

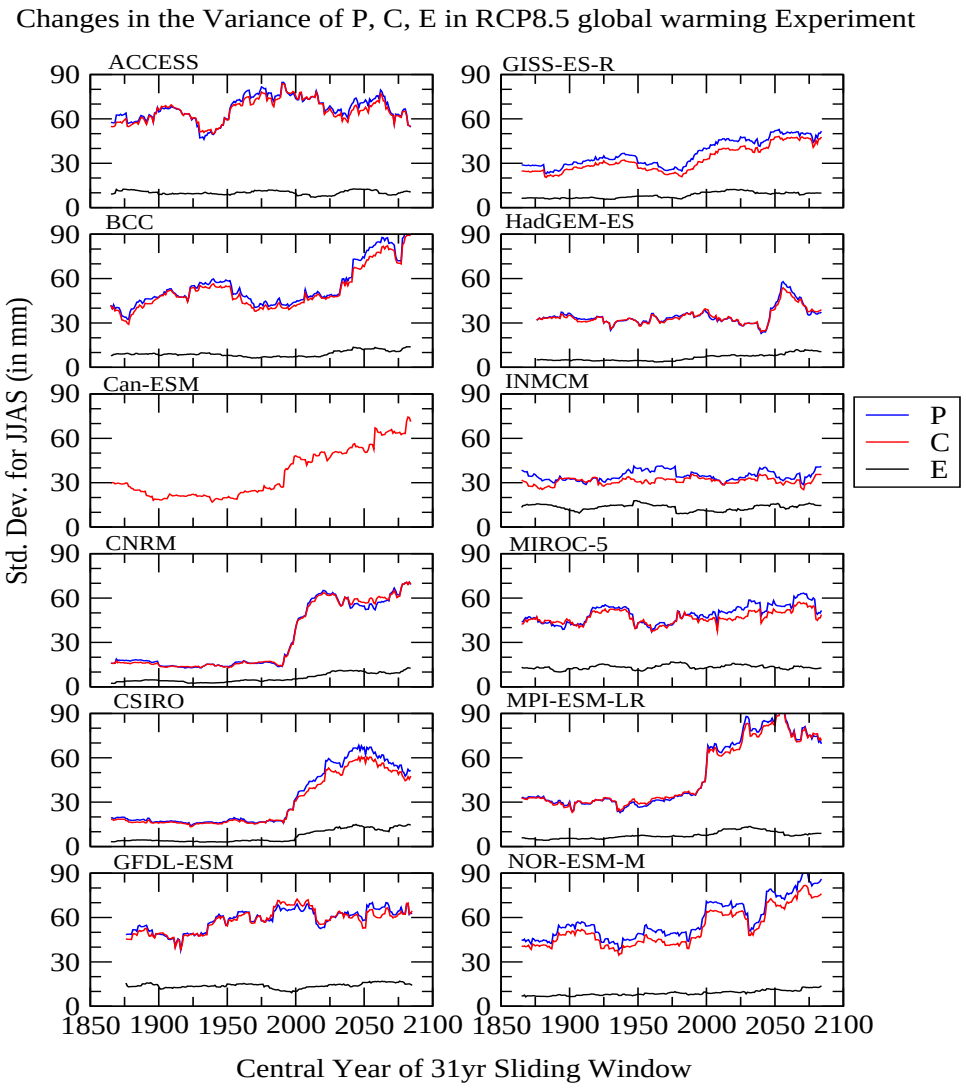

Figure 20 Future changes in the variance (time series from 1850 to 2100) of AWB components (P, C and E) (mm) (standard deviation is taken as a measure of variability) in different models for RCP8.5 scenario run. The blue lines denote standard deviation of precipitation in respective models; red lines indicate standard deviation of convergence: black lines indicate standard deviation of evaporation.

Table 1 Description of 12 Coupled climate Model Simulations used in the study

No.	Model	Institution	Country	Resolution	Time Period
1	ACCESS1-0	CSIRO	Australia	145x192x3072	185001-210012
2	BCC-CSM1.1	BCC	China	64x127x3072	185001-201212
3	CanESM2	CCCma	Canada	64x128x3072	185001-210012
4	CNRM-CM5	CNRM and CERFACS	France	128x256x3072	185001-210012
5	CSIRO-Mk3.6	CSIRO	Australia	96x192x3072	185001-210012
6	GFDL-ESM2M	NOAA GFDL	USA	90x144x3072	185001-210012
7	GISS- E2- R	NASA/GISS	USA	90x144x3072	185001-210012
8	HadGEM2-ES	MOHC	UK	145x192x3072	185001-210012
9	INM-CM4	INM	Russia	120x180x3072	185001-210012
10	MIROC5	AORI	Japan	128x256x3072	185001-210012
11	MPI-ESM-P	MPI-M	Germany	96x192x3072	185001-201212
12	NorESM1	NCC	Norway	96x144x3072	185001-210012

APCC TECHNICAL REPORT 2012-03

- An Assessment of Reliability in Climate Projections : Cloud Variation
- An Evaluation of the Ability of CMIP5 Multi-Models to Predict Interdiurnal Variability
- Climate Change Projection of South Asian Summer Monsoon
- The Role of the Western Pacific Oscillation Teleconnection Pattern

APEC Climate Center

12, Centum 7-ro, Haeundae-gu, Busan 612-020,
Republic of Korea
Tel: +82-51-745-3900 Fax: +82-51-745-3949
www.apcc21.org

비매품
9 788997 133387
ISBN 978-89-97333-38-7
ISBN 978-89-97333-35-6 (세트)